Aalto University
School of Science
Life Science Technologies

Laura Jukola

Hybrid positioning and magnetic field measurement system

Master's Thesis
Espoo, November 20, 2016

Supervisor: Professor Ilkka Laakso, Aalto University
Advisor: Professor Ilkka Laakso

Aalto University
School of Science
Life Science Technologies

ABSTRACT OF
MASTER'S THESIS

Author:	Laura Jukola		
Title:	Hybrid positioning and magnetic field measurement system		
Date:	November 20, 2016	**Pages:**	viii + 92
Major:	Biomedical Engineering	**Code:**	SCI3059
Supervisor:	Professor Ilkka Laakso		
Advisor:	Professor Ilkka Laakso		

Electromagnetic fields (EMF) exist everywhere, where there are electric currents. To alleviate public concern for the possible adverse health effects of EMF, it is important to evaluate the stray fields around sources, like household appliances, that people are exposed to every day.

Time-varying magnetic fields induce electric fields and currents to the human body. Authorities have established safety limits that help prevent health effects related to the induced currents such as stimulation of peripheral nerves or, in the worst case, stimulation of the heart muscle. People with implantable electrical devices such as pacemakers are even more vulnerable to the effects of EMF.

The goal of this thesis project was to create a hybrid magnetic field measurement and positioning system. With this system the strength of a magnetic field is measured and simultaneously the position and orientation of the magnetometer is tracked, which enables the measurement of the three-dimensional spatial distribution of a magnetic field. The system provides knowledge about how far from their sources the magnetic fields reach. The system utilizes Kinect sensor's skeletal tracking ability for the position tracking and iPhone's built-in accelerometer and gyroscope for evaluating the orientation of the magnetometer probe. The magnetic flux densities are measured with an induction coil sensor.

The spatial distribution of magnetic fields measured with this prototype system are visualized in Kinect's point cloud. The frequency range of the system is 1 Hz - 400 kHz with the current composition, but it can be expanded with a different magnetometer.

Keywords:	EMF, electromagnetic fields, Kinect, ICNIRP, magnetic field distribution
Language:	English

Aalto-yliopisto
Perustieteiden korkeakoulu
Life Science Technologies

DIPLOMITYÖN
TIIVISTELMÄ

Tekijä: Laura Jukola

Työn nimi:
Paikannukseen perustuva magneettikenttämittausjärjestelmä

Päiväys:	20. marraskuuta 2016	**Sivumäärä:**	viii + 92
Pääaine:	Biomedical Engineering	**Koodi:**	SCI3059
Valvoja:	Professori Ilkka Laakso		
Ohjaaja:	Professori Ilkka Laakso		

Sähkömagneettisia kenttiä muodostuu kaikkialla, missä on sähkövirtoja. Näiden kenttien mahdollisiin terveysvaikutuksiin liittyvän huolestuneisuuden vähentämiseksi on tärkeää selvittää lähteiden, kuten kodinkoneiden, ympärillä olevat kentät, joille ihmiset altistuvat lähes joka päivä.

Ajan suhteen muuttuva magneettikenttä indusoi ihmiseen sähkökenttiä ja -virtoja. Viranomaiset ovat asettaneet turvarajoja, jotka auttavat ehkäisemään näihin indusoituneisiin virtoihin liittyviä terveysvaikutuksia, kuten ääreishermoston stimulaatiota ja pahimmasssa tapauksessa sydänlihaksen stimuloitumista. Ihmiset, joilla on implantoitavia elektronisia laitteita, kuten sydämentahdistimia, ovat vielä herkempiä sähkömagneettisten kenttien vaikutuksille.

Tämän diplomityöprojektin tarkoituksena oli kehittää paikannukseen perustuva magneettikenttämittausjärjestelmä. Tällä järjestelmällä mitataan magneettikentän voimakkuus ja samanaikaisesti magneettikenttämittarin paikka ja asento, mikä mahdollistaa magneettikenttien kolmiulotteisen spatiaalisen jakauman mittaamisen. Järjestelmän avulla saadaan tietoa siitä, kuinka kauas lähteistä kentät ulottuvat. Järjestelmä hyödyntää Kinect sensorin kehonseurantaa paikantamiseen ja iPhonen sisäistä kiihtyvyysanturia ja gyroskooppia magneettikenttämittarin orientaation selvittämiseen. Magneettikenttiä mitataan induktiokelasensorilla.

Tällä järjestelmän protyypillä mitatut spatiaaliset magneettikenttäjakaumat visualisoidaan Kinectin point cloudia hyödyntäen. Järjestelmän taajuusalue on nykyisellä kokoonpanolla 1 Hz - 400 Hz, mutta sitä voi laajentaa käyttämällä erilaista magneettikenttämittaria.

Asiasanat:	Sähkömagneettiset kentät, Kinect, ICNIRP, magneettikenttäjakauma
Kieli:	Englanti

Acknowledgements

First I wish to thank my instructor and supervisor Ilkka Laakso, who first offered me the opportunity to work with this project and then provided me endless help and ideas.

A special thanks to my fellow worker Jonne Vähänissi for accompanying me in this project and tirelessly performing various measurements after another. And of course for building the famous test coils.

Thanks to Simo Särkkä for sharing his knowledge about inertial measurement units. Credit also needs to be given to other fellow workers for their help.

Finally I wish to thank my boyfriend Sampsa for unlimited patience and support (and Arduino ideas). Thanks also go to my family and friends for being there for me.

Espoo, November 20, 2016

Laura Jukola

Abbreviations and Symbols

EMF	Electromagnetic field
EU	European Union
FEM	Finite Element Method
ICNIRP	International Commission On Non-Ionizing Radiation Protection
IEC	International Electrotechnical Commission
IEEE	Institute of Electrical and Electronics Engineers, Inc
IMU	Inertial Measurement Unit
MEX	Matlab Executable
MEMS	Micro-Electromechanical System
MRI	Magnetic Resonance Imaging
RF	radio frequency
RFID	radio frequency identification
SDK	Software Development Kit
STUK	Radiation and Nuclear Safety Authority (Säteilyturvakeskus)
TMS	Transcranial Magnetic Stimulation
UDP	Universal Data Package
USB	Universal Serial Bus
v2	version 2

A	vector potential, area
B	magnetic flux density
c	speed of light
d	distance
E	electric field
f	frequency
H	strength of the magnetic field
I	electric current
J	current density

l	thickness
n	normal vector, amount
q	electric charge
r	radius
R	Hall coefficient
t	time
v	velocity
V	voltage
ε	induced voltage
θ	angle
μ	permeability
σ	conductivity
φ	phase
Φ	scalar potential
Φ_B	magnetic flux
ω	angular velocity

Contents

Chapter 1

Introduction

Electromagnetic fields (EMF) exist everywhere, where there are electric currents. These fields spread around household appliances, for example, and cannot be seen with the naked eye. For the sake of possible adverse health effects caused especially by time-varying magnetic fields, it is important to evaluate the stray electromagnetic fields around sources that exist almost everywhere in the human environment.[1] Another important reason, why the EMF must be investigated, is the electromagnetic compatibility. It refers to the safety of the environment for people who wear electrical implants, like pacemakers. (Ishida *et al*, 2016)

The amount of exposure to magnetic fields has in many cases been evaluated with measurements in a single point. The standard of the Institute of Electrical and Electronics Engineers, Inc (IEEE) suggests finding the maximum EMF strength over time and space in the locations, where people are exposed to these fields (IEEE, 2010). This was done in measurements performed by Radiation and Nuclear Safety Authority (STUK) evaluating the exposure levels at people's homes. The magnetic field was measured at several points, at a height of one meter from the floor, but only the largest value was chosen from each measurement area to describe the magnitude of the fields. (Nyberg and Jokela, 2006, Chapter 9)

A three-point measurement gives a better picture of the magnetic field distribution around the source. When measuring the magnetic field of household devices, STUK performed measurements at distances of 3 cm, 30 cm and 1 meter from the source (Nyberg and Jokela, 2006, Chapter 9). Laakso et al. evaluated the EMF distribution of a wireless power transfer system used for charging electric cars by measuring the magnetic field at different heights of 0.5, 1 and 1.5 meters (Laakso and Hirata, 2013). According to

[1] `http://www.who.int/peh-emf/about/WhatisEMF/en/`, Accessed: 10.11.2016

the standard of International Electrotechnical Commission (IEC) the exposure measurement is to be performed on all sides of the source accessible to the user. The IEC 62233 standard recommends a measurement distance of 30 centimeters, or 0 centimeters, if the user is in direct contact with the source during operation. The measurement distance has been established based on the approximate location of the user. If the source of the EMF can be moved, for example a small household appliance, the exposure has to be assessed around the source. (IEC, 2005)

The purpose of this thesis project is to create a system for the simultaneous measurement and positioning of time-varying magnetic fields. That way the three-dimensional magnetic field distribution can be evaluated. The resulting maps of magnetic field distributions can be used for the visualization of these fields around their sources and for more precise evaluation of the exposure.

This master's thesis project is part of a larger project, where the ultimate goal is to precisely evaluate electric fields induced to the human body by time-varying magnetic fields. This evaluation is performed by computer simulation. For these calculations a three-dimensional reconstruction of the measured magnetic field is required. The measurement system created in this master's thesis project can provide the required magnetic field data for the later reconstruction and the subsequent calculations.

1.1 Structure of the Thesis

Chapter two explains the fundamentals of electromagnetic fields (EMF) and their possible health effects. The chapter also introduces safety guidelines set by authorities to reduce the EMF exposure and gives examples of the sources of these fields. Chapter three narrates the tools required for the simultaneous positioning and measurement of magnetic fields. Chapter four describes the components of the measurement system created for this purpose. Chapter five contains the measurement results and chapter six the evaluation of the results and the overall performance of the measurement system. Conclusions are presented in chapter seven.

Chapter 2

Background

This chapter introduces the fundamentals of electromagnetic fields, describes the most frequent health effects related to these fields, introduces safety guidelines regarding EMF, gives examples of EMF sources and describes the method used for measuring three-dimensional magnetic field distributions.

2.1 Electromagnetic fields

Electromagnetic fields include electric and magnetic fields. A charged particle creates an electric field in its environment, while a magnetic field is generated by the movement of a charged particle, which means that a flowing current always generates a magnetic field. A direct current (DC) creates a static magnetic field and an alternating current (AC) a time-varying magnetic field. Both the electric fields and magnetic fields are vectors, meaning that they have both magnitude and direction.

The strength of an electric field can be expressed in volts per meter (V/m), whereas the strength of the magnetic field is expressed in amperes per meter A/m and the magnetic flux density in Teslas T. The connection between magnetic field strength and the magnetic flux density B is shown in equation 2.1

$$B = \mu_0 H \tag{2.1}$$

where $\mu_0 = 4\pi * 10^{-7}$ H/m is the permeability of vacuum.

When a conducting object is taken into an electric field, its charges will rearrange themselves on the surface of the object. This phenomenon is called electrostatic induction. A new secondary electric field is induced within the object, which further leads to currents being formed within an object in an electric field. The density of the currents is dependent on the conductivity

of the object as shown in Ohm's law in equation 2.2 (Young and Freedman, 2012)

$$J = \sigma E \tag{2.2}$$

where σ is the conductivity, J is the current density and E the electric field.

A varying magnetic field or, in other words, changing magnetic flux through a loop induces a voltage ε into that loop according to Faraday's law of induction

$$\varepsilon = -\frac{d\Phi_B}{dt} \tag{2.3}$$

where Φ_B is the varying magnetic flux. The greater the varying rate, or the frequency, of the magnetic field, the higher the induced voltage (Nyberg and Jokela, 2006, Chapter 2), (Young and Freedman, 2012). A time-varying magnetic field also induces a voltage into a conducting object in the field. A voltage always creates an electric field, which means that a varying magnetic field eventually induces an electric field. The electric field further creates eddy currents to a conductive object. The strength and density of the currents depend on the conductivity of the object according to equation 2.2. This whole phenomenon is called electromagnetic induction. (Nyberg and Jokela, 2006, Chapter 2) Electromagnetic induction also occurs when an object is moving in a static magnetic field. A varying magnetic field induces electric fields and currents also into a human body exposed to the field. (Nyberg and Jokela, 2006, Chapter 2)

A biological material such as tissue, for example, has nearly the same permeability as vacuum. Because of this a biological material, such as a human body, does not cause distortions to external magnetic fields. By contrast external electric fields with low frequencies are perturbed by the human body, because of its good conductivity. (WHO, 2007)

2.2 Evaluation of the induced internal electric fields

The induced internal electric fields and the current density are the most important features of human exposure to electromagnetic fields with frequencies up to 100 kHz. In the frequencies ranging from 100 kHz to 30 MHz the specific Absorption Rate (SAR) becomes an important feature measuring the amount of exposure. (Nyberg and Jokela, 2006, Chapter 3) The safety limits of ICNIRP and EU have been set for the internal electric field or induced internal current density (tables 2.1, 2.2, 2.3 and 2.4). The EU has established action levels for external electric and magnetic fields that help in the

estimation of the strength of the induced internal fields (tables 2.5 and 2.6). This is further explained in Section 2.4. The evaluation of the actual induced internal electric field is a challenging task. According to the Radiation and Nuclear Safety Authority of Finland (STUK), the internal electrical fields with frequencies ranging from 1 to 50 Hz can be measured. For the measurement of currents in the limbs a limb current meter can be used. This meter can be placed around the target limb or even the chest. (Nyberg and Jokela, 2006, Chapter 10)

The precise evaluation of the magnitude of the internal electric field can be performed by computer simulation. For these calculations a map of the varying magnetic field is required. (Laakso *et al*, 2015) When a human body is exposed to magnetic fields that vary in time, an electric field is induced within the body. This further causes internal eddy currents to form. The strength of the induced electric field and the currents is directly proportional to the frequency of the external magnetic field. (Nyberg and Jokela, 2006, Chapter 3)

The following is true for a magnetic field

$$B = \nabla \times A \tag{2.4}$$

where A is the vector potential of the field. (Laakso *et al*, 2015) The vector potential of the field can therefore be calculated from a measured magnetic flux density using volume integral

$$A = \text{"} \int_V B\text{"} \tag{2.5}$$

The details of this computation can be found in (Madsen *et al*, 2015). The electric field induced into a human body by a magnetic field can be calculated with the following equation

$$E = -\nabla\phi - \frac{\partial}{\partial t}A \tag{2.6}$$

where ϕ is the electric scalar potential of the field. (Laakso *et al*, 2015) The scalar potential can be solved from equation

$$\nabla \cdot \sigma\nabla\phi = -\nabla \cdot \sigma\frac{\partial}{\partial t}A \tag{2.7}$$

that has the boundary condition

$$n \cdot J = n\sigma E = \sigma n \cdot (-\nabla\phi - \frac{\partial}{\partial t}A) = 0 \tag{2.8}$$

where σ is the conductivity of the human tissue, J is the current density and n is the normal vector of the body surface (Laakso and Hirata, 2012). The boundary condition states that the current density outside the body surface must be zero. The induced electric field for the whole body can be solved using finite element method (FEM). (Ilvonen and Sarvas, 2007)

The strength of the induced internal field depends on the shape and size of the conductor, in this case the body, and also on the posture and the composition. On low frequencies, below 1 MHz, the human body works as a conductor but on high frequencies more like an insulator. The densities of the induced currents are highest in the armpits and groins, because there the direction of the currents changes rapidly. (Nyberg and Jokela, 2006, Chapter 2), (Laakso *et al*, 2015)

2.3 Biological effects of the electromagnetic fields

The wavelength of the electromagnetic radiation in the frequency range considered here is so long that it is non-ionizing radiation, which means that its energy is not sufficient for breaking molecular bonds [1].

The most frequent health effects that the exposure to electromagnetic fields causes is the stimulation of central and peripheral nervous systems, which occurs due to electric fields and currents induced inside the body by varying magnetic fields. The mechanism of this induction is explained more thoroughly in chapter 2.2. The threshold for the stimulation of myelinated peripheral nerve fibers is 4-6 V/m and for nerve fibers in the central nervous system around 10 V/m (ICNIRP, 2010). The exposure can also cause stimulation of sensory organs, for example eyes and ears (EU, 2013). The exposure of retinas to the EMF can result in phosphenes, which are faint flashes of light in the visual field. These occur due to the induction of electric fields into the retina. The threshold for phosphene induction is 50-100 mV/m at 20 Hz. (ICNIRP, 2010) Phosphenes no longer appear with frequencies higher than 100 Hz (Nyberg and Jokela, 2006, Chapter 4). The stimulation of the vestibular system can also lead to vertigo (EU, 2013). Because of this the exposure to varying EMF as well as movement in a static magnetic field can cause dizziness and nausea (IEEE, 2002).

Muscle cells become less easily stimulated than nerve cells. The worst case of muscle stimulation is the stimulation of the heart muscle, which could be life-threatening. At a 50 Hz frequency, arrhythmias occur if the strength of

[1] `http://www.who.int/peh-emf/en/`, Accessed: 20.8.2016

the electric field in the heart is above 10 V/m and if the internal electric field is stronger than 25 V/m, the heart may be driven into a life-threatening state of ventricular fibrillation. (Nyberg and Jokela, 2006, Chapter 4) The stimulation thresholds vary as a function of frequency. For the induction of phosphenes, the threshold is at its highest at 20 Hz. (ICNIRP, 2010) For the stimulation of myelinated nerves, the threshold starts increasing, when the frequency is higher than 1 kHz (Nyberg and Jokela, 2006, Chapter 4).

The exposure to EMF might have an adverse effect on brain functions such as visual processing and motor co-ordination. There might also be a connection between EMF and increased instances of leukaemia, especially in children. These health effects have not been used as a basis for the safety limits introduced in the next chapter, because the amount of research that has been done is insufficient to confirm these effects. (ICNIRP, 2010)

There is currently no reliable information concerning the long-term health effects of these fields (EU, 2013). The electromagnetic fields with sufficiently high frequency (above 100 kHz) can cause heating in tissues, because of the absorption of energy from the electromagnetic waves (EU, 2013). This thermal effect is measured with Specific Absorption Rate (SAR) (Nyberg and Jokela, 2006, Chapter 3).

Indirect effects of EMF are the interference with implantable electrical devices, such as pacemakers, and explosions or fire caused by sparks ignited by the induced fields or contact currents.

The penetration depth of the electromagnetic fields into the human body depends on the frequency of these fields. This project focuses on frequencies below 10 MHz. In this frequency range, the magnetic fields reach all of the body undistorted. (Nyberg and Jokela, 2006, Chapter 3)

2.4 Guidelines

The European Union established the directive 2013/35/EU for the regulation of exposure of employees to varying electric and magnetic fields at their working places in order to reduce the related possible adverse health effects. The safety levels in the directive are based on the guidelines established by the International Commission on Non-Ionizing Radiation Protection (ICNIRP) on limiting the exposure of humans to time-varying electromagnetic fields. (EU, 2013)

The basic restrictions of these guidelines are set so that below these limits the adverse health effects of the EMF do not occur. The basic restrictions set by ICNIRP are shown in Tables 2.1 and 2.2. These guidelines are given separately for occupational and general public exposure. The occupational

restrictions are higher compared to the public exposure, because the workers are exposed to EMF during working hours in controlled environment, where the employees have been notified about the possible health effects. More specific restrictions for different frequency ranges are set for the central nervous system (CNS) tissue in the head, which mostly consist of the brain. These ICNIRP guidelines only apply to the internal fields induced by external varying EMF and not to the electric fields that are induced by movement in a static field. (ICNIRP, 2010)

Table 2.1: Basic restrictions for internal electric field according to ICNIRP, occupational exposure

Exposure area	**Frequency range**	**Exposure limit (V/m)**
CNS tissue of the head	1 - 10 Hz	0.5/f
	10 - 25 Hz	0.05
	25 - 400 Hz	2×10^{-3} f
	400 Hz - 3 kHz	0.8
	3 kHz - 10 MHz	2.7×10^{-4} f
All other tissue	1 Hz - 3 kHz	0.8
	3 kHz - 10 MHz	2.7×10^{-4} f

Table 2.2: Basic restrictions for internal electric field according to ICNIRP, general public exposure

Exposure area	**Frequency range**	**Exposure limit (V/m)**
CNS tissue of the head	1 - 10 Hz	0.5/f
	10 - 25 Hz	0.01
	25 - 1000 Hz	4×10^{-4} f
	1000 Hz - 3 kHz	0.4
	3 kHz - 10 MHz	1.35×10^{-4} f
All other tissue	1 Hz - 3 kHz	0.4
	3 kHz - 10 MHz	1.35×10^{-4} f

The safety limits of the EU directive consist of basic restrictions and action levels. The basic restrictions of both ICNIRP and EU are based on the thresholds of biological effects, such as phosphene induction, and contain a safety margin. The biological effects and the corresponding thresholds were introduced in the previous section. The limits are set for the internal electric field in the human body.

The basic restrictions of the EU directive include two sets: health effect and sensory effect restrictions. These are shown in tables 2.3 and 2.4, respectively.

Table 2.3: Basic restrictions for internal electric field strength considering health effects according to EU

Frequency range	**Exposure limit (V/m)**
1 Hz - 3 kHz	1.1
3 kHz - 10 MHz	3.8 x 10^{-4} f

Table 2.4: Basic restrictions for internal electric field strength considering sensory effects according to EU

Frequency range	**Exposure limit (V/m)**
1 - 10 Hz	0.7/f
10 - 25 Hz	0.07
25 - 400 Hz	0.0028 f

The health effect safety limits protect people from thermal effects and muscle and neurostimulation that might occur above these limits. The limits for sensory effects protect against minor transient health effects such as phosphenes and stimulation of sensory organs. (EU, 2013) For example, in order to avoid both the adverse health effects and the sensory effects near an EMF sources with a frequency of 50 Hz, the strength of the internal electric field should remain below 140 mV/m.

The action levels of EU have been derived from the basic restrictions and are set for the external electric and magnetic fields. The action levels help to keep the strength of the induced internal electric field below the basic restrictions. If a person is exposed to external fields stronger than the reference level, an internal electric field stronger than the threshold for adverse health effects might be induced. (ICNIRP, 2010), (EU, 2013) Methods described in Section 2.2 are needed for more precise evaluation of the induced electric fields.

The action levels are presented as low and high levels and are set for both external electric and magnetic fields. Exposure below the high action level does not cause an internal electric field sufficiently strong for causing major health effects. However, phosphenes and other minor effects may occur. Limiting the exposure below the low action level maintains the internal field

so low, that also the minor sensory effects are avoided. (EU, 2013) The action levels for electric and magnetic fields are presented in tables 2.5 and 2.6, respectively.

Table 2.5: Action levels for electric fields, set by EU

Frequency range	E-field strength (V/m), low action level	E-field strength (V/m), high action level
1 – 25 Hz	2.0×10^4	2.0×10^4
25 – 50 Hz	$5.0 \times 10^5/f$	2.0×10^4
50 Hz – 1.64 kHz	$5.0 \times 10^5/f$	$1.0 \times 10^6/f$
1.64 – 3 kHz	$5.0 \times 10^5/f$	6.1×10^2
3 kHz – 10 MHz	1.7×10^2	6.1×10^2

Table 2.6: Action levels for magnetic fields, set by EU

Frequency range	Magnetic flux density (µT), low action level	Magnetic flux density (µT), high action level
1 – 8 Hz	$2.0 \times 10^5/f^2$	$3.0 \times 10^5/f$
8 – 25 Hz	$2.5 \times 10^4/f$	$3.0 \times 10^5/f$
25 – 300 Hz	1.0×10^3	$3.0 \times 10^5/f$
300 Hz – 3 kHz	$3.0 \times 10^5/f$	$3.0 \times 10^5/f$
3 kHz – 10 MHz	1.0×10^2	1.0×10^2

The magnetic field from 50 Hz sources, for example, should remain below 1 mT so that it can be considered safe, meaning that it will not induce adverse health effects nor sensory effects.

For EMF with frequencies higher than 10 MHz, the safety limits are based on the power and energy absorbed into tissues, which is measured with SAR. The absorbed power causes tissue heating. This thermal effect of the electromagnetic fields is present, when the frequency is higher than 100 kHz (ICNIRP, 2010), (Nyberg and Jokela, 2006, Chapter 4). The thermal effect should be considered in addition to the strength of the induced internal electric field, when the frequency exceeds 100 kHz.

In addition to observing the exceeding of the safety limits, also the frequency as well as the duration of the exposure need to be considered. What also effects the total amount of exposure is that the individual can be exposed to several EMF sources with differing frequencies (EU, 2013). Interference of fields with implantable devices can occur even if the strength of the fields is lower than the safety limits. Furthermore, children and pregnant women are generally more sensitive to the effects of EMF compared to other groups. (ICNIRP, 2010)

2.5 Sources of EMF

Electric and magnetic fields exist everywhere, where there is a flowing electric current: near power lines or electrical devices [2]. All household appliances, for example microwave ovens, create an electromagnetic field around them. The Earth has a static magnetic field, the strength of which in Finland is between 51 and 53.5 µT. The Earth's magnetic field does not cause any symptoms, because the threshold for physiological phenomena for static fields is 1 T. (Nyberg and Jokela, 2006, Chapter 9) The Radiation and Nuclear Safety Authority (STUK) has made a vast research on the sources of electromagnetic fields. Some sources and the frequencies of their magnetic fields are shown in table 2.7.

Electromagnetic fields can be divided into three classes based on their frequency: extremely low frequency fields (1-300 Hz), intermediate frequency fields (300 Hz - 10 MHz) and radiofrequency fields (10 MHz - 300 GHz) [3]. People are quite often exposed to the multi-frequency fields of electronic article surveillance systems in grocery stores or libraries. Their electromagnetic fields have multiple frequencies ranging from 73 Hz to 1 kHz or 10 to 20 MHz in radio frequency systems. The fields induced by railways, trains and power lines are sources of extremely low frequency electromagnetic fields that people are often exposed to, for example, while commuting. Magnetic Resonance Imaging (MRI) and Transcranial Magnetic Stimulation (TMS) devices create magnetic and electric fields that the human body is exposed to while under medical examination or therapy. In the MRI system there is a static magnetic field. Movement in this field can already cause sensory effects. The rapidly varying gradient fields and the essential RF-pulse are sources of time-varying magnetic fields. The exposure to the gradient fields can result in peripheral nerve or muscle stimulation. (Dempsey *et al*, 2002) The purpose of a TMS device is to stimulate the brain by delivering a magnetic field in it that further induces currents in the target area. This field typically has a frequency of 2.5 to 4.5 kHz.

Additionally, wireless power transfer systems are important sources of EMF, especially now that wireless chargers for electric cars and smart phones have become more popular. Wireless chargers could also be of use for implantable medical devices, because they would reduce the need for reoperation to change the batteries. (Bi *et al*, 2016) Transformers, power lines (Tong *et al*, 2016) and welding are sources for very low frequency (1-300 Hz) EM fields. The fields from the sources like induction heaters are in the fre-

[2] `http://www.who.int/peh-emf/en/`, Accessed: 20.8.2016
[3] `http://www.who.int/peh-emf/en/`, Accessed: 20.8.2016

quency range from 300 Hz to 100 kHz and cookers from 20-100 kHz (Nyberg and Jokela, 2006, Chapter 4), (Kos *et al*, 2011).

Table 2.7: Sources of electromagnetic fields (Nyberg and Jokela, 2006), (Kos *et al*, 2011),(Bi *et al*, 2016), (Waffenschmidt, 2011)

Source	Frequency
Vacuum cleaner	50 Hz
Electronic article surveillance system	73 Hz -1 kHz or 10-20 MHz
Induction cooker	20 -100 kHz
Induction heater (industry)	50 Hz - 3 MHz
Microwave oven	2450 MHz
MRI device	0 - 127 MHz
Power lines	50 Hz
TMS	2.5 - 4.5 kHz
Trains	50 Hz
Transformers	50 Hz
Wireless power transfer for phones	110 - 205 kHz or 6.78 MHz - 2.4 GHz
Wireless power transfer for vehicles	20 - 100 kHz

In this project we are mainly interested in the extremely low and intermediate frequency fields: frequencies between 1 Hz and 10 MHz.

2.6 Methods for measuring three-dimensional magnetic field distributions

This section describes some methods for evaluating the three-dimensional magnetic field distribution. The evaluation of magnetic field distributions from different sources is important, when it comes to health issues. It needs to be determined, whether the strength of the magnetic field of the source or the induced electric field exceeds the ICNIRP safety limits near the source. If the field strength is higher than the safety limit, then the minimum safety distance, where the human is no longer exposed to too strong fields, has to be determined. Another motivation for evaluating magnetic field distributions is its benefit to product development.

The measurement of the actual 3D distribution of electromagnetic fields brings more knowledge about the EMF. It can also bring relief to people when they get to know that the critically strong magnetic or electric field does not usually reach out very far from the source. The electromagnetic field

distributions around sources like household appliances are invisible. A measurement system for the 3D distribution of electromagnetic fields can help visualize these fields to average consumers (Sato *et al*, 2014). A common method for measuring the spatial distribution of a magnetic field is to use a two or three dimensional measurement grid (Madsen *et al*, 2015). The three dimensional distribution of a magnetic field can also be achieved computationally through simulation using for example the Finite Element Method (FEM) (Tong *et al*, 2016).

Sato et. al were among the first to measure three dimensional spatial magnetic field distribution by freehand scanning. During the measurement, the strength of the magnetic field is evaluated by moving a magnetic field sensor freely in the proximity of the source. Simultaneously the location of the probe is tracked in order to get the spatial distribution of the field. (Sato *et al*, 2012) The methods of Sato et. al included a system based on a Wiimote, which is the controller for the game console Nintendo Wii (Sato *et al*, 2012) and later on the Kinect sensor (Sato *et al*, 2014). In the Wiimote -project the magnetic field probe was equipped with an infrared marker, which was then tracked by using the Wiimote as an infrared camera (Sato *et al*, 2012). The Kinect-project utilized the sensors' built-in ability to track the hand of the operator (Sato *et al*, 2014). He et. al measured magnetic field distributions using optical tracking. They attached retroreflective markers to a magnetic field probe to track its position and orientation using an infrared camera, while performing freehand scanning of the magnetic fields. (He *et al*, 2016)

Freehand scanning enables the collection of a large amount of measurement points (He *et al*, 2013). The trajectory can be freely chosen and varied to whatever suits the particular source the best. User experience can be used for the improvement of measurement trajectories. (He *et al*, 2016) In this project the freehand scanning of the magnetic field and simultaneous positioning was used to achieve the magnetic field distribution.

2.6.1 3D reconstruction of a magnetic field

In order to be able to create a 3D reconstruction of a magnetic field, the strength and the direction of the field needs to be known everywhere. After a freehand measurement of the magnetic field, interpolation between data points is performed and subsequently the reconstruction is created. (Madsen *et al*, 2015) From this three dimensional model the vector potential of the field can be calculated using equation 2.5, which can then be used for the evaluation of the electric field induced into a human body by this field.

A successful reconstruction of a field requires a large amount of points and, as already mentioned, data about the direction of the field at every time

point. This requires knowledge about the orientation of the magnetic field probe at every measurement point.

Chapter 3

Measurement system

For the later reconstruction of the magnetic field and the following simulations of the induced internal electric fields, the magnetic field strength and simultaneously the position of the probe in real world coordinates need to be measured. In addition to that, the orientation of the magnetic field sensor needs to be acquired. All data is to be collected in real-time. This chapter introduces the tools required for real-time freehand measurement of magnetic field distributions. Position tracking can be performed with a Kinect sensor, the magnetic field strength can be measured with a magnetometer and the orientation can be achieved using inertial measurement unit (IMU) sensors.

3.1 Kinect sensor

The Kinect sensor is a device with an RGB camera and built-in depth sensing technology. The sensor was originally developed to be used in gaming. The first version of the sensor, Kinect sensor v1, was established in 2010 for Xbox 360. (Lachat and Macher, 2015) The idea behind the sensor is that players can interact with the games in a controller-free manner: the human body works as the controller. This is made possible with the built-in ability of the Kinect to track skeletons (Xu and McGorry, 2015), which is explained in detail in Section 3.1.4. The ability of the Kinect to produce 3D location data has caused researchers to develop several applications for the sensor. The idea of using this device for our project came from Sato et al., who measured the magnetic field distribution both with the help of a Wiimote and the Kinect sensor version 1. According to their study, from these two options the Kinect sensor was more accurate. The Kinect is capable of acquiring 30 frames per second, which makes it suitable for real-time tracking.

The Kinect sensor is a product of Microsoft. In this project the Kinect

Figure 3.1: Kinect sensor version 2 for Xbox One.

v2 that was released in July 2014 was used. The v2 is an improved version of the Kinect sensor with higher resolution and better quality of depth images compared to the earlier model. The new sensor has improved skeleton tracking abilities and lower noise level, especially in the depth images. Other improvements include a wider field of view, that is 70x60 degrees in the v2. The Kinect sensor v2 has two cameras, an RGB camera with full high definition (Full HD) resolution of 1920x1080 pixels and an infrared camera. The infrared camera has a resolution of 512x424 pixels and enables the acquisition of depthmaps of the environment. The distance measurement of the Kinect v2 is based on time-of-flight technology (TOF), which is further described in the next section. Microsoft announced the operative range of the sensor to be 0.5 to 4.5 meters [1] but Laukkanen claimed that the actual maximum range is much longer, even 9 meters. (Laukkanen, 2015) The sensor can detect the distance of the target from the sensor with an average error of only 2 mm (Yang *et al*, 2015). The technical details of the device are presented in table 3.1. The Kinect sensor is not suitable for detecting highly reflective or shiny surfaces, because the distance measurement is based on detecting reflected infrared beams. (Yang *et al*, 2015)

When it comes to system requirements, the Kinect sensor v2 is very de-

[1] `https://developer.microsoft.com/en-us/windows/kinect/hardware`, Accessed: 28.10.2016

Table 3.1: Technical details of the Kinect sensor version 2 (Laukkanen, 2015), `https://developer.microsoft.com/en-us/windows/kinect/hardware`

Color image resolution	1920 x 1080 (Full HD)
Depth and infrared image resolution	512 x 424
Field of view	70 x 60 degrees
Frame rate	30 Hz
Range	0.5 - 4.5 m
Accuracy in depth measurement	2 mm
Connection type	USB 3.0
Sound	Array of four microphones
Power	12V, 2,67A

manding. In order to function, it requires an USB3.0 port and its drivers and the separately downloadable Software Development Kit (SDK) are only supported by Windows 8 or newer. The Kinect version 2 is only supported as of Matlab 2016a (Laukkanen, 2015). The Software Development Kit contains ready-to-use functions for using the Kinect for a variety of purposes like tracking a skeleton.

Advantages of the Kinect include its low price and its ability to produce 3D location data. The sensor itself includes all three cameras, the color camera, and the combined infrared and depth cameras, required for 3D tracking.(Fleder *et al*, 2011) Figure 3.2 shows images acquired with the Full HD

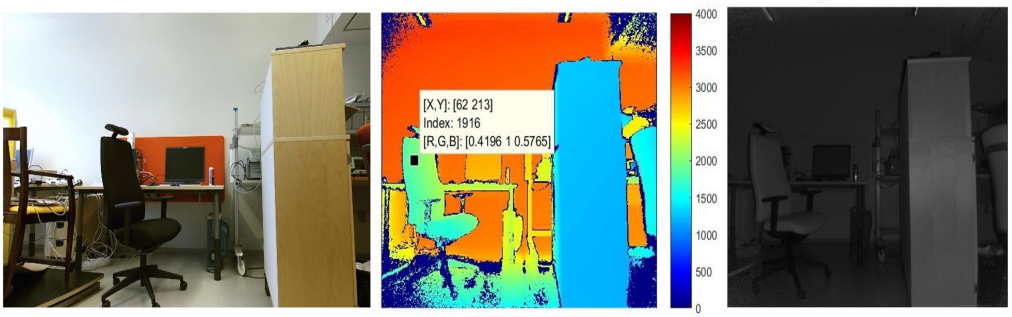

Figure 3.2: Images of the same scene from all three image sources of the Kinect: a) full-HD color image b) depth image c) infrared image

RGB camera, the depth camera and the infrared camera.

The Kinect has three different coordinate spaces: the color space, the depth space and the camera space. These are illustrated in Figure 3.4. The

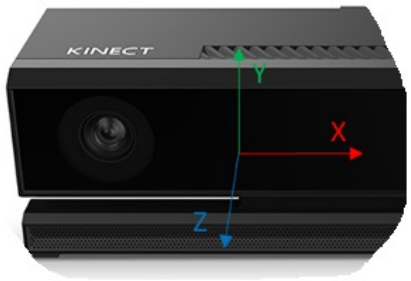

Figure 3.3: The axis of the Kinect camera space `https://msdn.microsoft.com/en-us/library/dn785530.aspx`

color space refers to two dimensional locations in the color image, given in pixels. The depth space similarly consists of 2D locations in the depth images, also given in pixels. A slight offset exists between the RGB camera and the infrared camera, which is why the view seen by the two cameras is different. The camera space is the 3D coordinate system of the Kinect. The origin is located in the center of the infrared camera and one unit in the system is one meter. The x-, y- and z-axis are oriented as shown in Figure 3.3. The SDK contains functions for mapping points from one of these described spaces into another. [2]

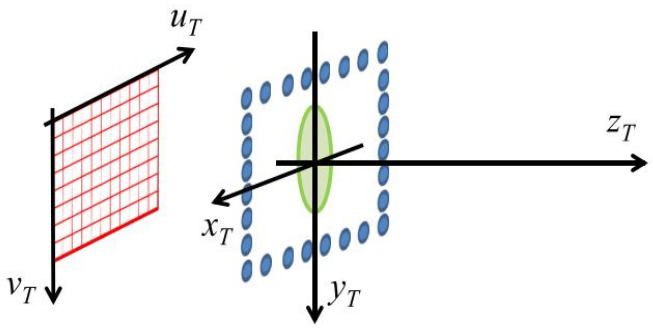

Figure 3.4: An image space, depth or color, with axes u and v and the camera space with axes x, y and z. (Dal Mutto *et al*, 2012)

[2] `https://msdn.microsoft.com/en-us/library/dn785530.aspx`, Accessed: 30.9.2016

3.1.1 Time-of-flight

The Kinect sensor utilizes time-of-flight (TOF) technology in its depth measurements. The technology is based on measuring the time it takes for an emitted light beam to travel forth and back to the sensor after being reflected from the target surface. The Kinect sensor v2 utilizes Continuous Wave modulated TOF, where the amplitude of the light is first modulated with a sinusoidal signal.(Dal Mutto *et al*, 2012) Then the sensor continuously illuminates the scene with this near infrared light that originates from its three infrared projectors. The emitted light beams undergo a phase shift while travelling from the emitters to the target and back. The phase shift occurs among others because of reflection related energy absorption.(Dal Mutto *et al*, 2012) Instead of directly measuring the time difference between the sent and received light beams, the sensor measures the phase shift, which is directly proportional to the distance travelled by the light. (Lachat and Macher, 2015), (Laukkanen, 2015) The distance from the sensor to the targets in the field-of-view can be calculated with the following equation:

$$d = \frac{\Delta\varphi}{4\pi f} \cdot c \tag{3.1}$$

where $\Delta\varphi$ is the phase difference, f is the modulation frequency and c is the speed of light. The depth image is a depthmap of the environment, a matrix consisting of 512x424 pixels that contain the acquired depth values or distances.(Lachat and Macher, 2015) The depth value is the perpendicular distance from the plane of the sensor, given in millimeters.

3.1.2 Point cloud

Point clouds of a scene can be created by combining the color information from the color images and the depth values from the depth images. Point clouds contain the 3D coordinates and the color values of the scene in the real-world coordinate system (camera space). An example point cloud acquired with Kinect is shown in Figure 3.5. Matlab version 2016a has its own function for making point clouds from the Kinect data called `pcfromkinect(depthImage, colorImage, alignment)`. It takes a depth image and a color image as a parameter. Because the color camera and the depth camera have a slight misalignment of 5 centimeters between them (Yang *et al*, 2015), they have to be aligned. 'depthcentric' or 'colorcentric' can be given as the 'alignment' parameter, which aligns the origo of the color

image with the origo of the depth image or vice versa. [3]

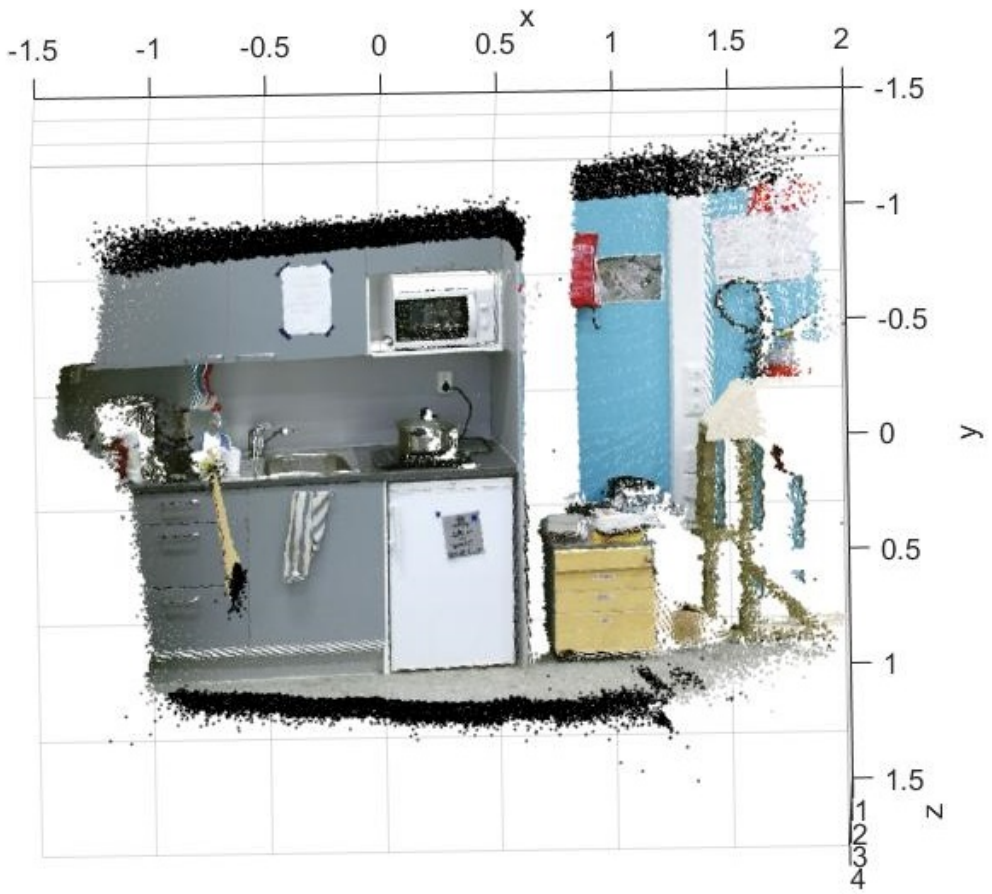

Figure 3.5: A point cloud created with the Kinect

The depth image is taken from a single point of view, which is why only the distance of the nearest object can be mapped. Objects behind the nearest object are occluded (Laukkanen, 2015). This causes areas of missing data to appear in the point cloud.

[3] `https://se.mathworks.com/help/vision/ref/pcfromkinect.html`, Accessed: 3.6.2016

3.1.3 Skeletal tracking

The Kinect sensor has a built-in ability of tracking a human body, more precisely its skeleton. The Kinect sensor v2 is able to simultaneously track up to six skeletons. (Lun and Zhao, 2015) The skeleton data is included in the depth images and contains the 3D coordinates of 25 body joints: the spine base, the middle of the spine, the spine at the shoulder level, the neck, the head, the left and right shoulders, the left and right elbows, wrists, hands and tips of the hands depicting fingers, two thumbs, the left and right knees, ankles and feet and left and right portions of the hip. (Xu and McGorry, 2015) The skeleton tracking ability is depicted in Figure 3.6, where the red dots represent the 25 body joints. The indexing and locations for the joints are shown in Figure 3.7.

The sensor has also been trained to track hand gestures (Lun and Zhao, 2015). The green circles in Figure 3.6 indicate that the user's hands are open. A red circle means closed hand or closed fist and a blue circle indicates a hand gesture called lasso. The body joints in the middle of the green circles are the hand joints. The skeleton is a mirror image of the user, therefore the right hand joint is on the right, like in reality. The coordinates of the joints are automatically given in the Kinect's camera space as 3D real-world coordinates. [4]

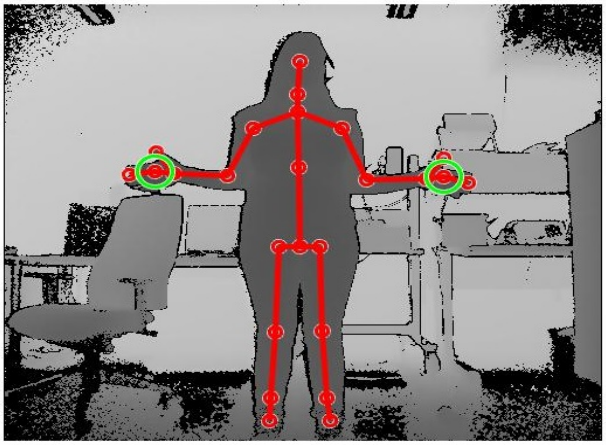

Figure 3.6: The skeletal tracking

The skeleton tracking, or the body tracking, ability of the Kinect sensor was developed utilizing machine learning, segmentation and probabilities.

[4] `https://msdn.microsoft.com/en-us/library/dn785530.aspx`, Accessed: 1.10.2016

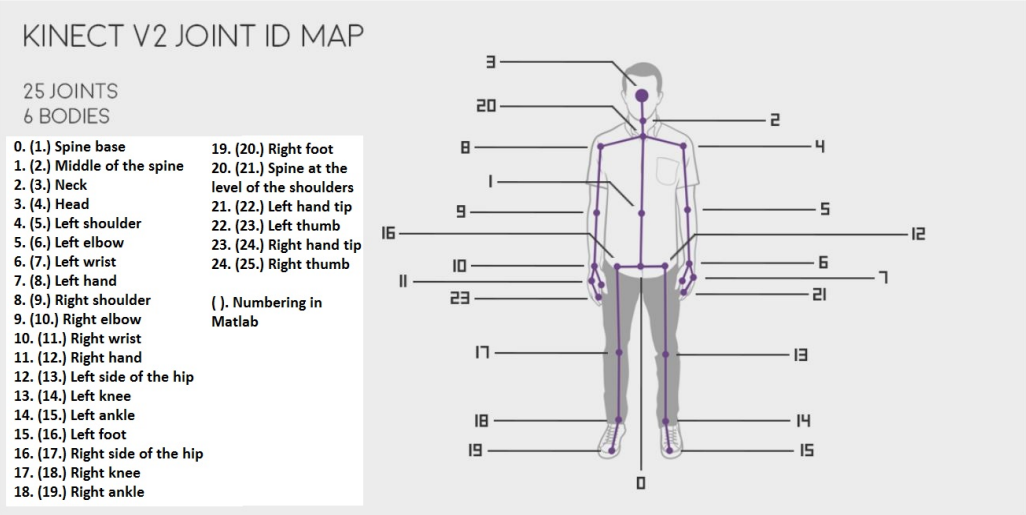

Figure 3.7: Body joint indexing `https://vvvv.org/documentation/kinect`, accessed: 16.6.2016

Shotton et al. created a training set consisting of synthetic and real depth images of human bodies in order to train the Kinect for body tracking. In both the synthetic and real training images different body shapes, sizes and poses were included. In the synthetic images also the shape and size of clothing and hair were varied. This is needed, because the skeleton tracking needs to work for all individuals with diverse outfits. (Shotton *et al*, 2013)

3.2 Gyroscope and accelerometer

In addition to the 3D coordinates of the magnetic field sensor, we also need to obtain the orientation of the sensor. Inertial measurement units, or accelerometers and gyroscopes, can be used for this purpose.

An accelerometer can be used for the measurement of acceleration in three axis, the x-, y- and z-axis. When there is no acceleration present, an accelerometer can measure its angle with respect to gravity. In other words, it can be used as an inclinometer. (Luinge and Veltink, 2005) Normally, however, also acceleration generated by movement of the accelerometer is present. Therefore the acceleration measured by the sensor is a sum of gravitation and this movement related acceleration. (Sarkka *et al*, 2015) One restriction with the accelerometer is that it does not give information about the rotation around the vertical axis. Therefore with the combined Kinect

sensor and accelerometer five degrees of freedom can be measured: translation along the x, y and z axes and rotation around the x and y axes. For the sixth degree of freedom, the rotation around the z-axis, we need data from a gyroscope.

A gyroscope measures the angular velocity it is experiencing around three axes, which helps it to detect rotation around different axes. Orientation θ (a change in angle) can be achieved from the angular velocity ω by integration as shown in equations 3.2, 3.3 and 3.4 (Luinge and Veltink, 2005)

$$\omega = \frac{d\theta}{dt} \tag{3.2}$$

$$\omega dt = d\theta \tag{3.3}$$

$$\theta = \int \omega dt \tag{3.4}$$

Because there is always some random noise present in the measurements, the gyroscope data has an accumulation error. Because of the noise, the sensor appears to have angular velocity, even though in reality it is kept still. This causes the inclination angle to grow linearly with time. This phenomenon can be reduced by calibrating the gyroscope data.(Woodman, 2007)

Both the accelerometer and the gyroscope produce errors. The errors of the accelerometer arise from the fact that besides measuring the acceleration caused by gravitation, it also measures the acceleration caused by movement. An accelerometer-gyroscope combination is needed in order to produce reliable orientation information.(Starlino, 2009) A Kalman filter can be used to combine the accelerometer and gyroscope data to reduce errors and increase the accuracy of the orientation measurement. The Kalman filter utilizes the difference in the inclinations given by the two sensors as an error model and produces the corrected inclination. (Luinge and Veltink, 2005), (Sarkka *et al*, 2015)

Both sensors perform measurements in their own coordinate system. The reading needs to be transformed into the real-world coordinates or the global coordinates with the help of direction cosine matrices.(Sarkka *et al*, 2015)

3.3 Magnetometers

The strength of a magnetic field can be measured with sensors called magnetometers. Most of these sensors actually measure the magnetic flux density. (Lenz, 1990) The magnetic field sensors can be divided into two categories based on whether they can measure static fields or time-varying fields. They

can also be divided into scalar and vector sensors. Scalar sensors measure the total magnitude of the magnetic field, while vector sensors can measure one or more separate components of the magnetic field and determine the direction of the field.(Lenz and Edelstein, 2006)

The most of the health effects related to electromagnetic fields arise from the induction of internal electric fields and currents. This only occurs with time-varying magnetic fields, which is why this project focuses on measuring them and not the static fields. For the later three dimensional reconstruction of the measured field both the direction and the strength of the field need to be measured, which means that all three components of the field are to be evaluated. This can be accomplished with a vector sensor. Time-varying magnetic fields can be measured with the following vector sensors: search coil - or induction coil -sensors, fluxgate sensors and Hall-sensors. The hybrid positioning and magnetic field measurement system is meant to measure fields of a variety of sources with greatly varying strengths and frequencies, which sets requirements for the frequency and field strength range of the magnetometer used in this project.

3.3.1 Hall-sensor

A Hall-sensor, illustrated in Figure 3.8, consists of a flat conductor or semiconductor with electrodes on top (Macintyre, 1999). The functioning of the

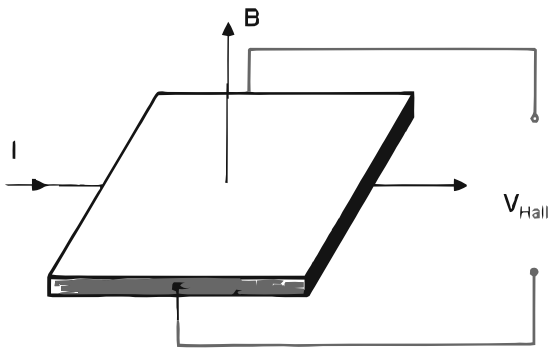

Figure 3.8: A Hall-sensor (Lenz and Edelstein, 2006)

Hall-effect probes is based on Lorentz force. When a material that has an electric current flowing through it is put into a magnetic field, the magnetic

field acts on the moving charges, electrons, with a force known as Lorentz force

$$F = -q(E + v \times B) \tag{3.5}$$

where q is the charge of the electrons, B is the magnetic flux density of the magnetic field influencing these particles and v is the velocity of the electrons. (Macintyre, 1999) Lorentz force will cause electrons to curve from their path and accumulate on one side of the plate of the Hall-sensor they are flowing in. This will create a voltage across the material, which is called the Hall-effect. The created voltage, or Hall voltage, is proportional to the magnitude of the magnetic field, as shown in the following equation

$$V = \frac{R}{l} IB \tag{3.6}$$

where R is a factor, which describes the properties of the Hall-sensor material, l is the thickness of the sensor plate, I is the current and B the magnetic flux density. (Tumanski, 2011)

Hall-sensors excel at measuring high field strengths of static or time-varying fields ranging from 0.1 mT to 30 T, with frequencies between 0 Hz and 100 MHz (Macintyre, 1999).

3.3.2 Fluxgate magnetometer

Fluxgate magnetometers consist of two coils wound around a ferromagnetic core. The coils are referred to as the primary and secondary coils. Alternating current flows through the primary coil, which gives rise to a time-varying magnetic field that further induces an alternating electric current into the secondary coil. The phase and intensity of this secondary current are measured. An external magnetic field causes changes in the secondary current and by analysing these changes, the magnitude and the orientation of the external field can be evaluated. [5] A three-component fluxgate sensor (Figure 3.9) consist of three coil pairs enabling the measurement of the three, x, y and z, components of the magnetic field. An advantage of a fluxgate magnetometer is its ability to measure static magnetic fields in addition to alternating fields. [6] The magnetic field range of a fluxgate sensor is from 0.4 µT to 0.5 mT (Macintyre, 1999) and the frequency range from 0 Hz to 10 kHz (Lenz and Edelstein, 2006).

[5] `http://www.geol-amu.org/notes/m10-1-8.htm`, Accessed: 2.11.2016

[6] `http://www.emfs.info/what/measuring/`, Accessed: 10.10.2016

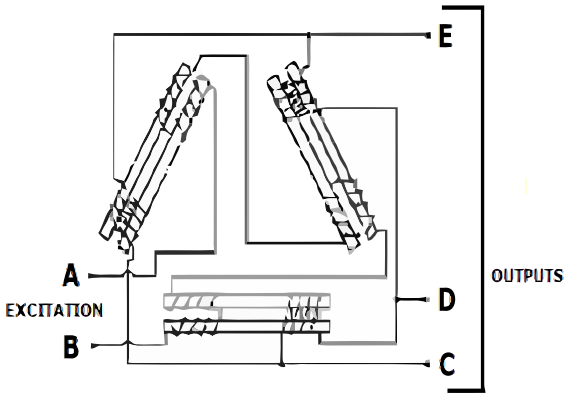

Figure 3.9: A fluxgate sensor (Lenz and Edelstein, 2006)

3.3.3 Induction coil sensor

Induction coil sensors are capable of measuring alternating magnetic fields with magnetic flux densities between 0.1 pT and 1 kT and frequencies ranging from 0.1 Hz to 1 MHz (Macintyre, 1999). An induction coil sensor consist of one to three rectangular or circular coils and measures the voltage induced in them. Figure 3.10 depicts the signal in the x coil of a magnetometer probe. A transfer function or the sensitivity of the coil is the relation between the

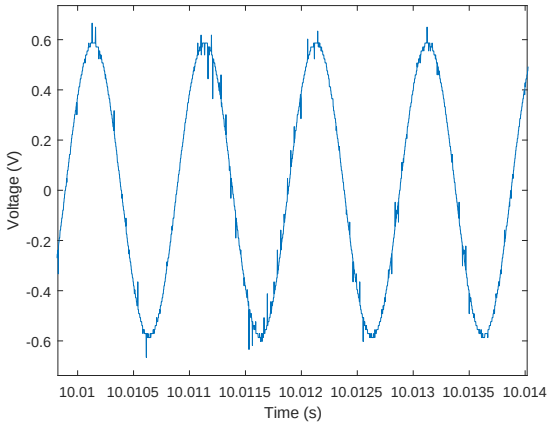

Figure 3.10: The signal of the x coil, while measuring a magnetic field with a frequency of 1 kHz

magnetometers input, the magnetic flux density, and output, the measured voltage (Robbes, 2006). The transfer function of induction coils comes from the Faraday's law of induction

$$V = -n\frac{d\Phi_B}{dt} = -nA\frac{dB}{dt} \tag{3.7}$$

where Φ_B is the magnetic flux and B the magnetic flux density flowing through the coil, n is the amount of turns in the coil and A is the area of the coil. Hence, the sensitivity of a search coil is dependent on the amount of turns in the coil, the area of the coil and the rate of change of the magnetic flux density through the coil. For a sinusoidal magnetic field the following is true (Kännälä *et al*, 2009)

$$\frac{dB}{dt} = 2\pi f B \tag{3.8}$$

According to the equations above, induction only occurs, if an alternating magnetic flux density passes through the coils, which is why induction coil sensors are not suitable for the measurement of static magnetic fields (Tumanski, 2007).

Coil sensors can only measure the magnetic flux density that is perpendicular to their axis. In order to measure all three components of the magnetic field, three orthogonal coils are required. Orientation of the coils for a three-axis magnetic flux density measurement is shown in Figure 3.11. A magnetic field sensor consisting of three orthogonal coils is referred to as an isotropic coil. (Nyberg and Jokela, 2006, Chapter 10)

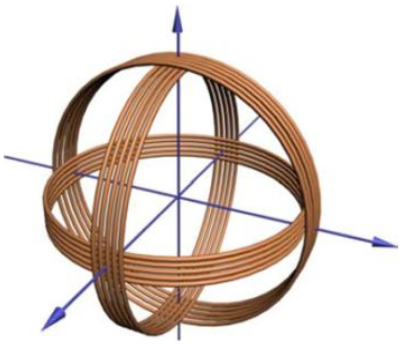

Figure 3.11: Orientation of orthogonal coils for three-axis magnetic field measurement(Tumanski, 2007)

The corresponding magnetic field components can be calculated from the voltages induced in the coils using the transfer function characteristic to the

probe. Then the total magnetic flux density can be calculated from the magnetic field components using root-sum-of-squares addition:

$$B = \sqrt{B_x^2 + B_y^2 + B_z^2} \tag{3.9}$$

A disadvantage of using a search coil sensor is its sensitivity to movement. The induction of voltage into the measurement coils occurs because the flux through the coils change. A change in the magnetic flux density can also occur due to coil movement or rotations, which means that these affect the meter readings. (Lenz and Edelstein, 2006) The frequencies lower than 30 Hz should be filtered out from the magnetic field data in order to remove the effect of the voltages induced by movement in Earth's magnetic field. [7]

Compared to a Hall-sensor a search coil sensor has a wider range of field strengths it can detect (Tumanski, 2007), while the Hall-sensor has a wider frequency range of these two. The fluxgate sensor has the smallest frequency and magnetic field range of these three sensor types. Considering the magnetic field strength range, the search coils and the Hall-sensors are most suitable for this project. The larger magnetic field and the suitable frequency range of the induction coil sensor makes it the best candidate out of these two.

[7] `http://www.emfs.info/what/measuring/`, Accessed: 10.10.2016

Chapter 4

Implementation

This chapter explains the implementation of the different parts of the measurement system in data collection. The components of the system are shown in Figure 4.1.

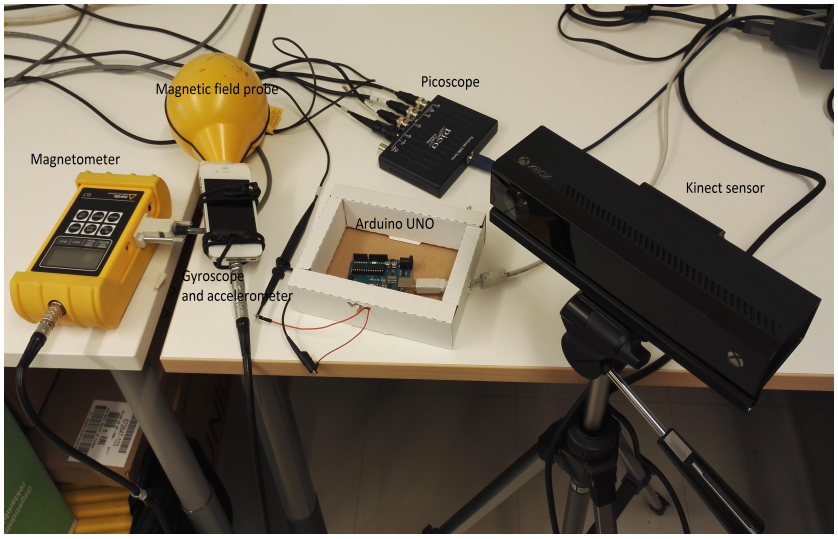

Figure 4.1: Components of the hybrid positioning and magnetic field measurement system

4.1 Magnetic field data collection

In this project the ELT-400 Exposure Level Tester of Narda, a three-axis induction coil sensor, was used for the measurement of the magnetic fields.

This probe has a frequency range of 1 Hz-400 kHz. [1] Its technical details are explained in table 4.1. This project focuses on measuring the low-frequency fields, below 10 MHz, so the magnetic field -device in question is suitable for this purpose. The ELT-400 consists of an external isotropic 100 m2 magnetic field probe, which contains three orthogonal sensor coils, and the actual measurement device, as shown in Figure 4.2 a. [2] Figure 4.3 shows

Figure 4.2: a) Narda's ELT-400 Exposure Level Tester for magnetic fields and b) PicoScope 2406b from Picotechnology

the arrangement of the coils relative to the probe. The coils can be matched with the real-world axes by positioning the probe in the way described in Figure 4.3: the probe must be tilted to an angle of exactly 35.3 degrees and held in this position. Then the x- and z-axis are perpendicular to each other and at an angle of 45 degrees relative to the central axis of the measurement device and the y-axis is perpendicular to the floor.

[1] `http://www.narda-sts.us/pdf_files/DataSheets/ELT400_DataSheet.pdf`, Accessed: 14.4.2016

[2] `http://www.narda-sts.us/pdf_files/DataSheets/ELT400_DataSheet.pdf`, Accessed: 14.4.2016

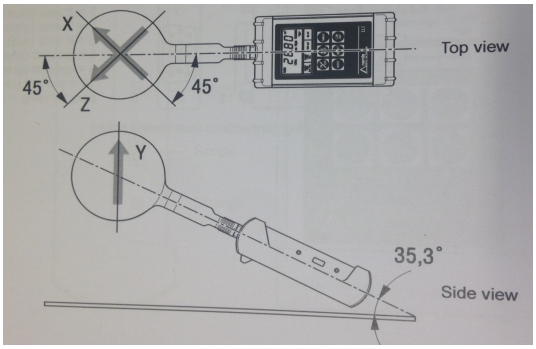

Figure 4.3: The orientation of the measurement axis of the ELT-400. (Narda, 2011)

Table 4.1: Technical details of the ELT-400 Exposure Level Tester (Narda, 2011)

Probe	Isotropic 100 cm^2
Frequency range	1 Hz - 400 kHz
Resolution	1 nT
Measurement uncertainty	4%
Connection type	D-SUB15 plug

The ELT-400 has an exposure mode, where it automatically compares the measured magnetic field value to the ICNIRP safety guidelines. The value is given as a percentage of the exposure limit. The probe also has different modes for the measurement of magnetic field strength as shown in table 4.2. The probe can measure field strengths with a maximum of 80 mT. In addition to Narda's magnetic field probe, we had a probe home-made by

Table 4.2: Field strength measurement modes of the Narda-probe. (Narda, 2011)

Mode	320 µT		80 mT	
Range	LOW	HIGH	LOW	HIGH
Overload limit	32 µT	320 µT	8 mT	80 mT
Typical noise level	60 nT	320 nT	10 µT	80 µT

STUK at our disposal, presented in Figure 4.4.

The probe consists of three orthogonal coils, each composing of 40 loops of copper wire and has a diameter of 30 mm (Kännälä *et al*, 2009). Because of its small size, it bests the Narda-probe in measuring the magnetic fields from small sources. It also fits in the hand of the user, which improves the tracking result with Kinect. However, this probe is primitive: it, for example, lacks noise protection and is therefore prone to disturbances. In the comparison of the signals from the Narda probe and STUK's probe in Section 5.3 can be seen that the signal of the latter contains far more distortion.

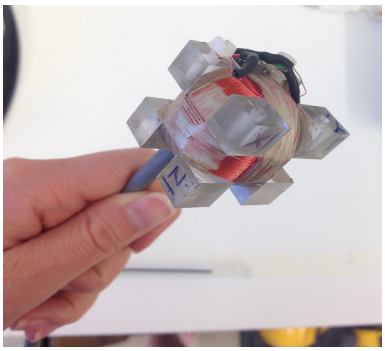

Figure 4.4: STUK's hand-made magnetic field probe

4.1.1 PicoScope

The readings from all coils of a magnetic field probe can be separately acquired by using an USB oscilloscope. This is referred to as operating the probe as an active probe. In this case we used a four-channel PicoScope 2406B shown in Figure 4.2 b. Its technical details are given in Table 4.3. Acquiring all three components of the magnetic field strength is necessary for our applications, because this information is needed for the 3D reconstruction of the magnetic field.

Table 4.3: Technical details of the PicoScope 2406B `https://www.picotech.com/oscilloscope/2000/picoscope-2000-specifications`

Bandwidth	50 MHz
Memory (streaming mode)	100 MS
Maximum sampling rate (streaming mode)	9.6 MS/s
Channels	4
Connection type	USB

The PicoScope has two different data collection modes: the block mode and the streaming mode. In the block mode the scope collects a block of samples. Data is collected continuously in the streaming mode, where the collection time is limited by the sampling rate and the scopes memory. In

this project we use the streaming mode, because we need to collect data in real-time. In streaming mode the scope can collect 25 megasamples of data, because its 100 MS memory is divided for all four channels.[3]

In order to start the measurement of the magnetic field, a trigger is sent to the PicoScope through an adjacent channel. The trigger is produced into channel D with an Arduino UNO microcontroller (Figure 4.5), which causes a pulse greater than the triggering threshold to occur. The microcontroller is connected to an USB port in the computer. The trigger pulse is initiated with a signal from Matlab. The collection of magnetic field data starts with the trigger, which enables the synchronization of the magnetic field data with location and orientation data.

Figure 4.5: Arduino UNO microcontroller

The maximum amount of samples the PicoScope 2406b can collect is about 25 000 000 due to its limited memory. Because of this the maximum sampling rate of the PicoScope decreases with an increasing measurement duration. Table 4.4 shows the maximum sampling rates associated with different measurement durations, when data is collected from all four channels of the PicoScope using the streaming mode. For example in a measurement lasting 50 seconds the sampling rate is 500 kHz and 250 kHz in a measurement with a duration of 100 seconds.

The maximum sampling rates set limits to the frequency range of the magnetic field for our measurements. The Nyquist theorem states that the sampling rate must be at least twice the frequency of the signal (Heinzel *et al*, 2002). The magnetic field data is collected into PicoScope 6, Pico Technology's own program, that allows modification of the measurement duration, the triggering threshold and the sampling rate, with the above-explained restrictions.

The data can be saved as a Matlab .mat-file that contains data arrays from all channels and the time intervals between sampling points. PicoScope 6 also offers an option of measuring a frequency spectrum in real-time in its spectrum state.

[3] `https://www.picotech.com/oscilloscope/2000/picoscope-2000-specifications`, Accessed: 20.08.2016

Table 4.4: Maximum sampling rates of the PicoScope for different measurement durations, when data is collected from all four channels

Duration	Sampling rate
1 s	4.167 MHz
5 s	2.404 MHz
10 s	2.404 MHz
20 s	1.25 MHZ
50 s	500 kHz
100 s	250 kHz
200 s	125 kHz

4.2 Collecting positional data with the help of Kinect's body tracking

The position of the magnetic field probe at each time point is required for acquiring the field distribution. In this project, the skeleton tracking ability of Kinect was utilized for tracking the magnetic field probe during the measurement of magnetic field distribution. The Kinect sensor is built for the skeleton tracking purpose and its SDK includes ready-to-use algorithms for skeletal data collection, which makes this method easier to implement compared to the time consuming and complex ways of image processing that are described in the next section. When a magnetic field probe is in the user's right or left hand, its approximate center is tracked as the right or left hand joint, which enables the acquisition of the 3D coordinates of the probe in real time. This way each measurement position of the magnetic field is acquired with an average accuracy of 25 mm (Xu and McGorry, 2015). The tracked probe is illustrated in Figure 4.6. Sato et al. also used the hand tracking method of the Kinect sensor for measuring the 3D distribution of electromagnetic fields, indicating that this method is suitable for this project (Sato *et al*, 2014).

Figure 4.6: Using the Kinect's skeletal tracking to track the magnetic field probe.

A Kinect toolbox called Kin2 created by J.R.Terven contains several demo functions for using the Kinect. These utilize Kinect's own functions found in Kinect's Software Development Kit published by Microsoft. The functions in the SDK have been written in C++ and they are called in Matlab algorithms trough Mex-files in J.R.Terven's examples. A Mex-file is a Matlab Executable that enables the calling of functions coded with C, C++ or Fortran from Matlab. The general structure of these algorithms is shown in Figure 4.7. Terven's toolbox provides easy access to the Kinect functions in the SDK. (Terven and Córdova-Esparza, 2016)

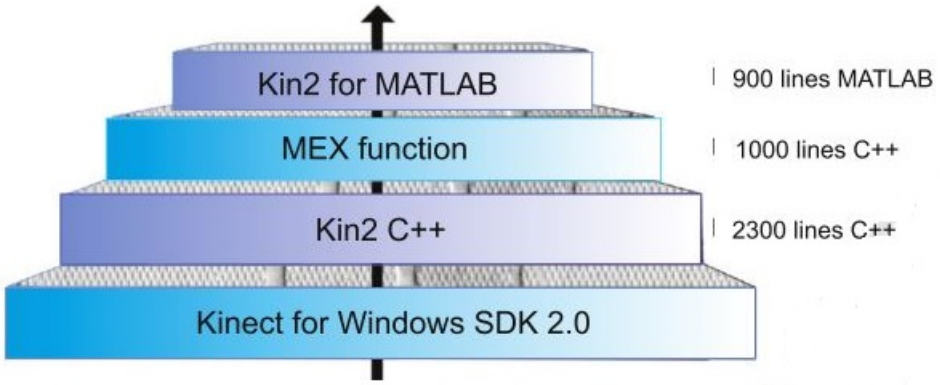

Figure 4.7: The structure of Terven's algorithms for the Kinect version 2 Matlab interface. (Terven and Córdova-Esparza, 2016)

J.R.Terven also created a Body Demo -function for skeleton tracking, where first a Kinect C++ -object is created. It has to be defined, which data sources the object needs to use. Different sources of Kinect include the color, depth and the infrared camera and body source for body tracking. In the body tracking case, color, depth and body sources are needed. The Kinect object is created and initialized for the gathering of data or frames from these sources. Color and depth frames are first acquired from the sensor,

for the later visualization of the skeleton data. The body data is stored in a Matlab structure 'Bodies' with fields position, orientation, tracking state, left hand state and right hand state. These are collected individually for every frame. The fields are all arrays and the position, orientation and the tracking state arrays contain one column for each of the 25 joints. The tracking state -array contains information about how well each joint was tracked. Different states are NotTracked = 0, Inferred = 1 and Tracked = 2. (Terven and Córdova-Esparza, 2016) The hand states refer to the different hand gestures as explained in Section 3.1.3. The orientation data is used for the correct replication of the body pose while drawing the skeleton and is given as quaternions for each joint or bone relative to the parent bone.

The final step of the body tracking is the use of the body data for drawing the skeleton of the tracked user on both the color and depth frames. Each frame achieved from Kinect is displayed in Matlab, so that the success of the body tracking can be monitored. The BodyDemo keeps running and acquiring frames until the user commands it to stop.

The measurement algorithm in this project is built around J.R.Terven's Body Demo. In the algorithm, the location data of the right hand, or optionally the left hand, is collected from each frame into an array. The right hand joint is joint number 12, as can be seen from Figure 3.7, so the location data for this joint is in the `Bodies.Position` array in column 12. Positional data for the left hand joint is in column 8. The skeleton drawn in each frame helps to monitor, whether the tracking is proceeding well.

4.3 Other methods for tracking the probe

The initial approach for tracking the magnetic field probe was by ways of image processing. These possibilities were studied and they appeared to be problematic. The aim was to be able to first detect and track Narda's probe with known, quite distinctive, color and shape. The probe is depicted in Figure 4.2 a. The 3D-position of the probe needed to be tracked in each frame acquired by the Kinect sensor.

The detection of known objects is a problem of computer vision (Han *et al*, 2015) that can be solved for example by image processing. An image processing -based approach for object tracking is mentioned in many sources, when it comes to performing object tracking with Kinect: segmentation [4], background subtraction (Han *et al*, 2015) and point cloud processing (Fleder

[4] `http://web.stanford.edu/class/cs231a/prev_projects/Gbrantner_Lstelzner_Mtroesch_cs231a_final_report.pdf`, Accessed: 15.10.2016

et al, 2011) are brought out. The possibilities of segmentation, training an object detector and point cloud processing were studied in this project.

4.3.1 Segmentation

A conventional approach for object detection is segmentation. One way is to segment objects in the image by color and this way extract all, for example yellow, components from the image. The resulting black and white image contains all the yellow objects. The problem here is that the image may contain several yellow objects (other than the object of interest) with varying sizes. In order to extract the desired object, objects of certain size such as too small objects, can be excluded from the black and white image using the Matlab-function `bwareopen(image, size)`. The problem here is that the size of the object of interest, the probe, also varies in the images as a function of its distance to the Kinect-sensor, which may lead to false detection or exclusion of the object of interest from the image. Additionally, this method only works for detecting an object with distinctive color, which makes it unsuitable for tracking the smaller magnetic field probe used in this project, because it is not characterized with a distinguishing color.

4.3.2 Training an object detector in Matlab

There is a built-in function in Matlab's Computer Vision System Toolbox for training a cascade object detector called `trainacascadedetector` for the detection of objects of interest. In order to create a reliable detector, training data is needed, in other words, hundreds of images, where the object of interest has been highlighted. A set of these so called positive images can be created with Matlab's Training Image Labeler. The training also requires a set of negative images, where the target is not present. [5] The amount of training data needed for this purpose is so large, that it makes this method time consuming. Figure 4.8 shows the result of tracking Narda's probe in Kinect's color image with a cascade detector, that was trained using a dataset of 41 positive images and 25 negative images. The detector marks off the detected probe with a box. The center point of the detected probe is approximately in the center of the box, the coordinates of which need to be determined. The points' x- and y-coordinates are given in pixels, thus there is a need to map this color image point to the camera space in order to get the real-world 3D coordinates. This can be done with Kinect's own function `mapColorPoints2Camera` found in the SDK.

[5] `http://se.mathworks.com/help/vision/ref/traincascadeobjectdetector.html`, Accessed: 10.4.2016

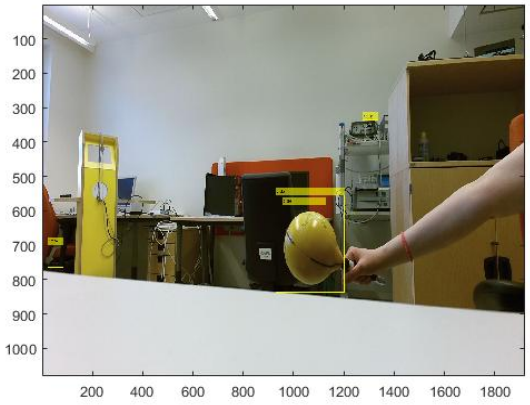

Figure 4.8: A succesful detection of the probe with the cascade detector.

Figure 4.8 depicts a successful detection of the magnetic field probe with a newly trained cascade detector. However, as can be seen from the image, also falsely tracked targets are present. Therefore the detector is not sufficiently accurate, which is due to a inadequate amount of training images.

Using the cascade trainer has limitations. The approach is very time consuming and the training data has to be collected as well as the training performed separately for the two probes in use. Again if in the future there would be a need to use a new probe in addition to the ones that are currently in use, it would force the training process to start all over again, including collecting new training data. This is because the functioning of the cascade detector is based on the appearance and the features of the probe. The detector is only capable of detecting the object of interest in a single orientation, meaning that a separate detector needs to be trained for each orientation of the object. [6] However, during the measurements in this project, the orientation of the probe varies. Because of these above-mentioned reasons this approach is not good for the purposes of this project.

4.3.3 Point cloud processing

Another method for tracking the probe is using point clouds created from Kinect's color and depth images. Matlab's Computer Vision System Toolbox contains functions for fitting shapes into point clouds. Since Narda's magne-

[6] `http://se.mathworks.com/help/vision/ref/traincascadeobjectdetector.html`, Accessed: 10.4.2016

tometer probe is shaped like a sphere, the `pcfitsphere` -function is fitting. [7] Initially the average RGB-color value of the probe is calculated by hand from a color image. An initial point is then determined from the point cloud by finding a point, whose RGB-value is the closest to the average color of the probe. Then points that reside within the diameter of the probe, about 11 centimetres from the initial point, are selected and the sphere is fitted to these points. The center point of the sphere model is the 3D location of the probe. The advantage of this approach is that it gives as a result the 3D position of the center of the probe in real-world coordinates (Kinect's camera space).

A challenge associated with the sphere fitting is the fact that the color of the wall or light coloured furniture is too close to the average color of the probe. In addition to that, the color of the probe varies with the lighting conditions. This leads to the selection of wrong points from the point cloud and finally to a failure in sphere fitting. A possible solution for this problem would be to coat the probe with a textile that has a more unique color to make it stand out from the background. The exclusion of the background from the point cloud by thresholding further enhances the outcome.

Fitting a sphere to a point cloud, however, is not a suitable approach for the detection of the smaller probe, since it is square-shaped. A further mismatch between this approach and the detection of the hand-made probe lies in the fact that there is no ready-to-use function for fitting a cube into the point cloud. The same problem arises with other non-spherical probes as well.

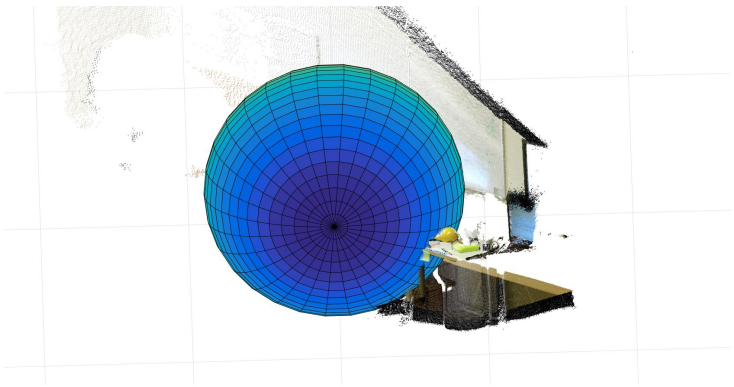

Figure 4.9: Failure in point cloud sphere fitting.

[7] `http://se.mathworks.com/help/vision/ref/pcfitsphere.html?searchHighlight=pcfitsphere`, Accessed: 16.4.2016

Figure 4.9 represents a failure in fitting a sphere to the point cloud. The sphere was not successfully fit to the location of the probe, most likely because of the too small difference between the average color of the wall in the background and the probe. This led to the sphere being fit to the wall.

4.4 Collection of orientation data

In this project an iPhone 4S that has a three-axis Micro Electro-Mechanical System or MEMS accelerometer and a three-axis MEMS gyroscope was used as the source of orientation data (Niu *et al*, 2012). iPhone 4S also contains a teslameter. The smartphone is attached to the magnetometer probe as shown in Figure 4.10.

The internal sensors of the iPhone track the orientation of the probe. The axis of the gyroscope and accelerometer are as shown in Figure 4.11 a, when the phone is lying on the table on its back.

Figure 4.10: The smart phone iPhone 4S collects data about the orientation of the magnetic field probe.

In order to align the axes of the smart phone with those of Kinect, the measurement has to be started in a position, where the axes are aligned: when the user is facing the Kinect sensor, the probe-smart phone combination has to be pointing upwards with the screen of the phone facing backwards. The later orientations are given relative to this starting orientation. The data from the inertial sensors is collected by an application called Sensor Streamer and sent to the computer as User Datagram protocol (UDP) packages over the wireless local area network (WLAN). A screenshot of the application is shown in Figure 4.11 b. This data is collected from the mobile phone's built-in accelerometer, gyroscope and teslameter with a sampling frequency ranging from 1 Hz to 100 Hz. The collection of the UDP packages is performed in a Python-code, which is called from the measurement algorithm. The readings are saved to a text file. A time stamp attached to the data enables the synchronization of the inertial measurement unit (IMU) sensor data with the location data received from the Kinect and the magnetic field data.

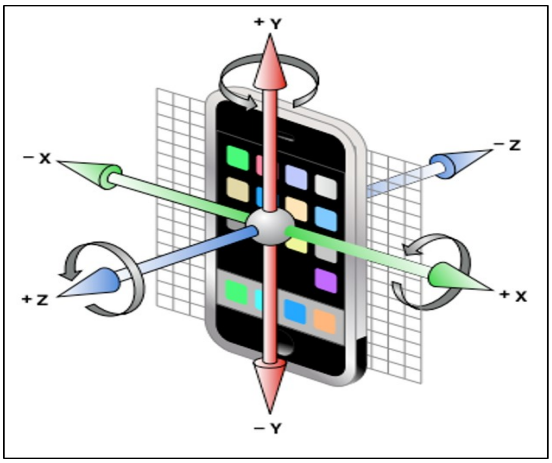

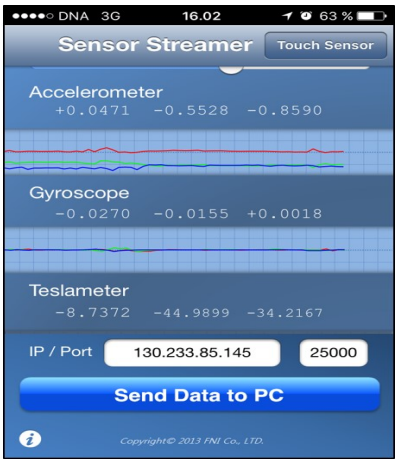

Figure 4.11: a) The axis of the iPhone's gyroscope and accelerometer, when the phone is lying on the table on its back. `https://developer.apple.com/library/content/documentation/UserExperience/Conceptual/DesigningExpandedAdUnits/FeaturesforExpandedAdUnits/FeaturesforExpandedAdUnits.html`, Accessed: 15.10.2016 b) Phone application Sensor Streamer created by Wavefront for collecting the data from the smartphone's gyroscope, accelerometer and teslameter.

4.5 Measurement

The measurement system for simultaneous evaluation of the magnetic field and the position and orientation of the probe consists of the Kinect sensor, a magnetic field probe, iPhone 4S's internal accelerometer and gyroscope, a PicoScope, an Arduino microcontroller and a computer. The components of the system are shown in Figure 4.1.

In the measurement system, the magnetic field sensor is held in the hand by the user. The mobile phone, that collects orientation data through its IMU sensors, is attached to the probe measuring the magnetic field. The block diagram of the system is presented in Figure 4.12. The magnetic field readings are measured with the magnetic field sensor and collected in PicoScope 6 through the PicoScope. The Kinect sensor is monitoring the scene and tracks the location of the probe in the user's hand in 3D. In the data collection process, the user must stand in front of the Kinect sensor, in its visual field. The best accuracy for positioning and best result in visualization with the point cloud can be achieved, if the measurement target is approximately in the center of the sensor's field of view with the distance to the sensor being between 0.5 and 3 meters (Yang *et al*, 2015). When the measurement

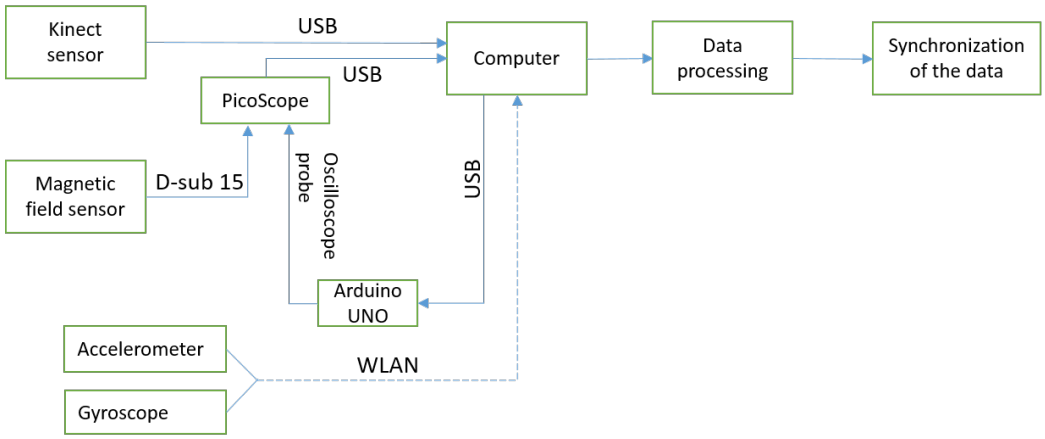

Figure 4.12: The system that measures magnetic field strength as function of location.

algorithm is run, the first color and depth frames appear. The algorithm then waits for a mouse button click from the user. If the user presses the left mouse button, the next frame is acquired. The tracking only starts if the right mouse button is clicked, which enables checking if the tracking of the probe seems successful and if other settings are in place prior to starting the collection of positional data. The right button click initiates the running of the Python code, that collects the orientation of the probe through the measurement, further initiates the real-time collection of the position of the probe in the user's hand, simultaneously collects the time stamp of the first data point and triggers the microcontroller to send a signal to the PicoScope in order to start the measurement of the magnetic field. When the data collection has started, the actual measurement is performed by moving the probe freely around the source until the measurement time set in the PicoScope runs out. The measurement process is illustrated in Figure 4.13.

A good measurement time is found to be between 20 - 200 seconds, depending on the desired trajectory complexity. With these durations, PicoScope's sampling rate is between 1.25 MHz and 125 kHz, as shown in table 4.4. Since the sampling rate is dependent on the measurement duration, the frequency of the target also affects the length of the chosen time span. According to the Nyquist theorem, the sampling rate has to be at least double the frequency of the measured field (Heinzel *et al*, 2002). Considering this, 20 second duration enables the measurement of frequencies up to 625 kHz and a 200 second measurement only up to 62.5 kHz. However, the actual limiting factor for the frequency range in the current configuration of the

system are the probes, which limit the maximum frequency to 400 kHz. The actual amount of measurement points of both position and magnetic field strength is limited by the frame rate of the Kinect sensor, which is about six frames per second with the current algorithm.

Figure 4.13: Measurement process.

The location data collected by the Kinect is saved to a .mat file along with a point cloud taken from the measurement scene for later visualization purposes. The magnetic field raw data is saved in a separate .mat file from the PicoScope program and the orientational data and its timestamp are stored in separate text files.

4.6 Data processing

After the measurement, both the magnetic field and the orientation data need to be processed.

4.6.1 Magnetic field data processing

First the magnetic field data can be down sampled to reduce noise. Then the data is windowed so that it matches the time interval of the frames acquired with the Kinect sensor, because the amount of samples collected by the Kinect and PicoScope differ dramatically. Hann and flat top window functions are used for the windowing. Flat top window is good at preserving

the amplitude of the signal, which is vital when the strength of the field with different frequencies is to be determined, but causes spectral leakage meaning the widening of the peak in the frequency domain. Hann window has reduced spectral leakage compared to the flat top window, which makes it more suitable for the cases, where adjacent frequencies have to be distinguished from each other. (Heinzel *et al*, 2002) The window represents a certain time interval, which in this case is the Kinect's frame interval. The frequency distribution is achieved for each window by performing Fourier analysis in order to get the frequency distribution of the signal in each time point. These data processing phases are done separately for the data from each of the three coils of the probe. The total RMS voltage is calculated separately for each frequency and for each time point and the result is transferred to magnetic flux density with methods explained below for both probes.

Both magnetic field probes used in this project are induction coils, meaning that they measure the voltage induced in their coils by a time-varying magnetic field. The measured voltages need to be transferred to magnetic flux densities. In the case of Narda's probe the B_x, B_y and B_z components of the magnetic field can be calculated from the corresponding voltages by dividing with the sensitivity, also known as the probe factor, that can be calculated with the following equation

$$sensitivity = 800mV/overloadlimit \tag{4.1}$$

The output voltage is 800 mV, when the magnetic field strength equals the overload limit. The overload limit varies with the field strength mode that has been used according to Table 4.2. (Narda, 2011)

From the equations 3.7 and 3.8, the following transfer function can be solved for STUK's probe

$$B_i = \frac{V_i}{2\pi^2 f r^2} \tag{4.2}$$

where V_i is the voltage induced in coil i, f is the frequency of the measured magnetic field and r is the radius of the probe.

4.6.2 Magnetic field frequency spectrum

The magnetic field data usually contains several frequencies. Therefore the frequency distribution of the source has to be analysed, in order to be able to evaluate the strength of the magnetic field actually originating from the source of interest. The frequency spectra and spectrograms calculated for each Kinect time point are visualized and used for the frequency analysis. An example frequency spectrum is shown in Figure 4.14 a and a spectrogram

in Figure 4.14 b. The total magnetic field is a sum of all magnetic fields present. In the measurements, the frequency with the highest amplitude in the spectrum is expected to be the frequency of interest or the dominant frequency of the source. In the case of Figure 4.14 a, the highest peak is at the frequency of 1 kHz, which is the frequency of the measurement target. This is shown also in the spectrogram as the brightest stripe. A spectrogram displays the frequency distribution of the magnetic field as a function of time throughout the measurement.

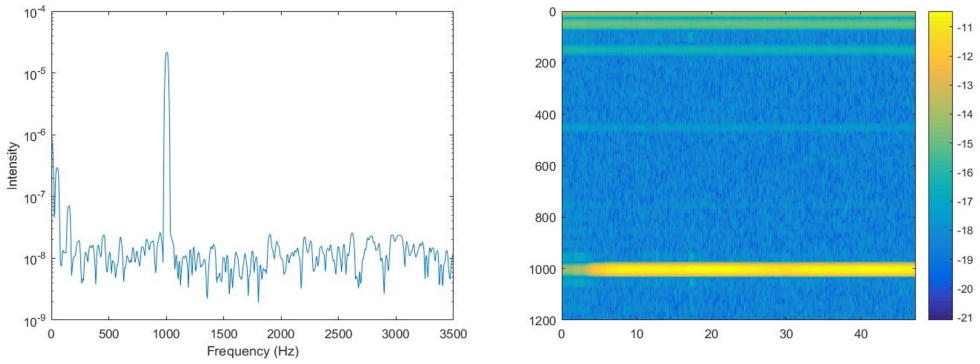

Figure 4.14: a) Frequency spectrum and b) spectrogram of a magnetic field with a 1 kHz frequency

In some cases, the peak of the main frequency is wide, which means that the dominant frequency is slightly changing. This is characteristic to the main magnetic field of an induction cooker and a surveillance system, as shown in Figure 4.15. In these cases, the total dominant magnetic field

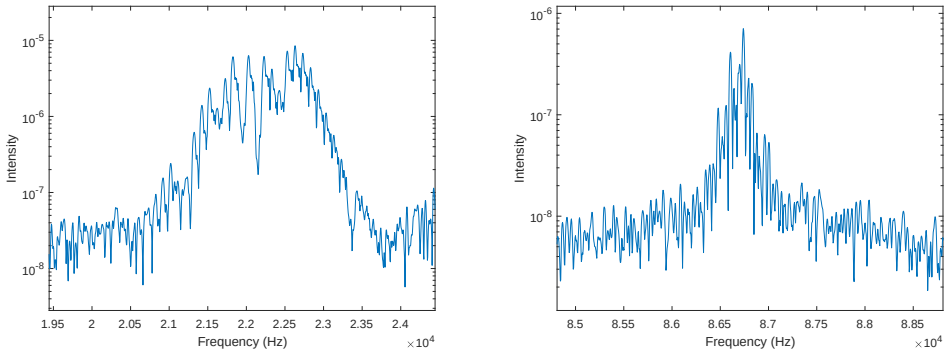

Figure 4.15: The wide peaks of the main frequency of a) and induction cooker b) a surveillance gate

is calculated by summing all the amplitudes comprising the highest peak. This represents the theoretical situation, where all the fields with adjacent frequencies would be at their peak at the same time, making it the worst possible case considering the amount of exposure.

4.6.3 Processing of the orientation data

Calibration of the gyroscope data must be performed before the collection of the accelerometer and gyroscope sensor readings in order to avoid the accumulation error. The accumulation error can be fixed with a simple calibration: gyroscope data for a stationary phone must be recorded and the mean calculated from that data is the calibration value that must be reduced from all measurements. The calibration must be repeated prior to every measurement, because the zero point of the gyroscope shifts, which causes the calibration values to change between measurements.

The actual inclination of the probe at every time point is achieved by combining the information given by the gyroscope and the accelerometer using a Kalman filter. A direction cosine matrix as well as the quaternions for the orientations during each time point are calculated. The direction cosine matrix is then used for transforming the orientation given in the sensors' coordinate system into the real-world coordinate system. The real-world coordinate system in this case is the coordinates of the starting position and, in case they were aligned, Kinect's coordinate system (camera space). The final orientation data now contains quaternions for each time point, telling the orientation of the probe relative to the starting position.

Chapter 5

Results

5.1 Gyroscope calibration

The gyroscope needed to be calibrated before every measurement. Figure 5.1 shows the effect of calibration on the accumulation error in the gyroscope. In this experiment the phone was lying on the table in the xy-plane along the x-axis facing east. The phone was then rotated 360 degrees rather slowly in the xy-plane and set back to its original position. However, because of the accumulation error, the final position differs from the initial position and instead of being aligned with the x-axis, the phone is tilted approximately 45 degrees relative to the x-axis in its final position. It can be seen from the figures, that the final position of the phone in the calibrated data is closer to the initial position, which states that the accumulation error is clearly reduced due to calibration. Here the phone is almost aligned with the x-axis.

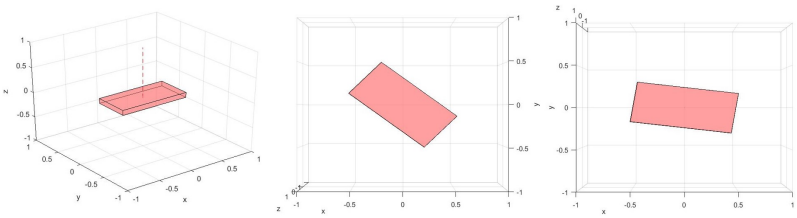

Figure 5.1: Results of the calibration of the gyroscope. Figure a shows the initial position of the phone during the measurement and figures b and c show the final position in the non-calibrated and in the calibrated data, respectively. These images are taken from an algorithm that repeats the orientations of the phone according to the time series of quaternions.

5.2 Results of tracking the probe with Kinect

The Kinect sensor is used for tracking the magnetic field probe in the user's hand. Failures in tracking occur in some cases, as shown in Figure 5.2. To enhance the tracking results, the probe must be held quite close to the body. If the arm is extended, the probe ends up too far from the body, which causes tracking failures similar to the one depicted in Figure 5.2 c. It also must be made sure that the user stays in the field of view of the sensor, otherwise serious failures in body tracking occur as shown in Figure 5.2 f.

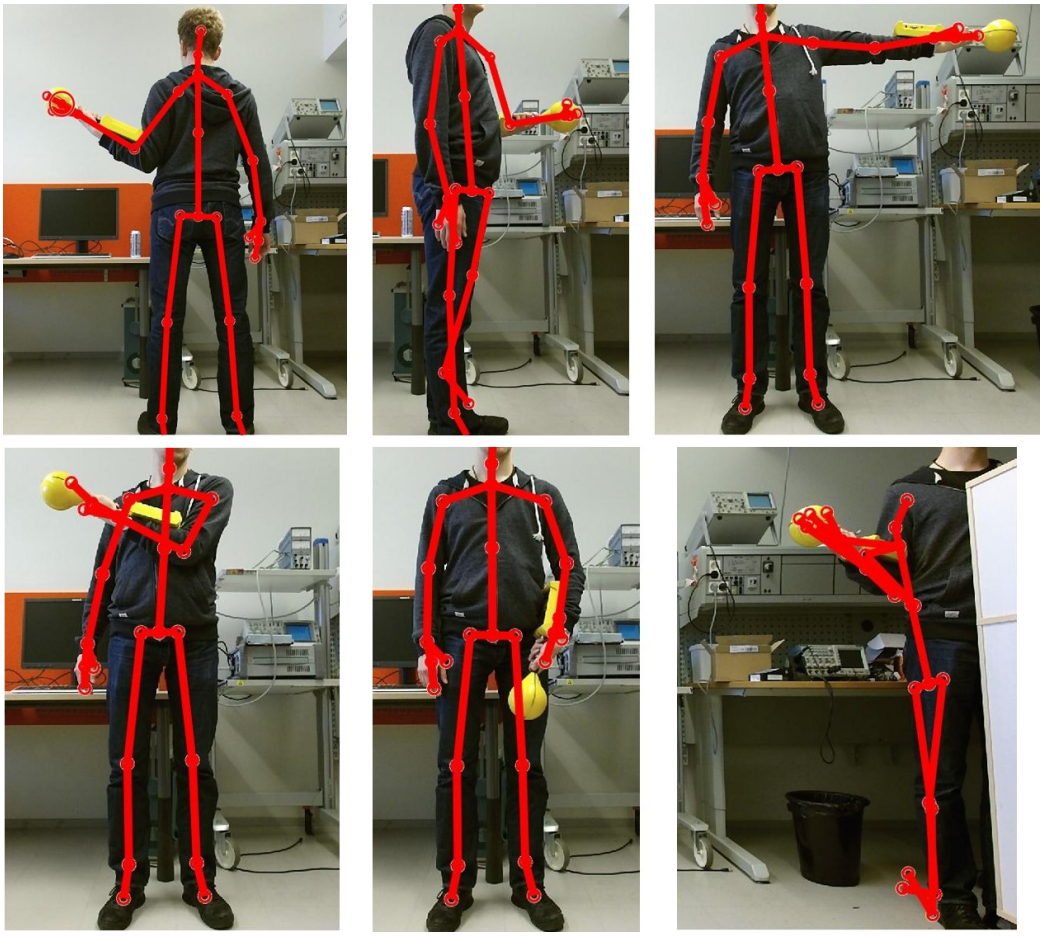

Figure 5.2: Results of tracking the magnetic field probe with Kinect

Figures 5.2 a and b depict how the tracking works also when the user's back is facing the sensor or the user is standing sideways. From Figure 5.3 can be seen that the tracking of the probe is also successful, when the user is

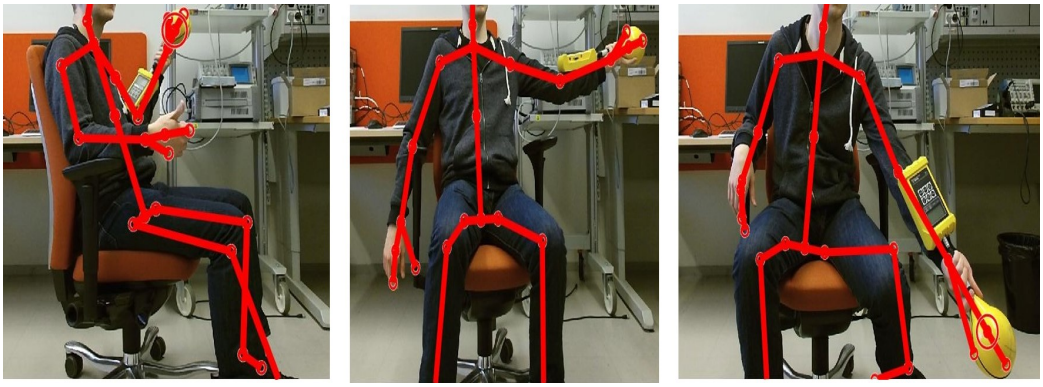

Figure 5.3: Results of tracking the magnetic field probe while sitting

sitting. Even further the pose, where the user's hand is extended, no longer cause failures, as shown in Figures 5.3 b and c.

The tracking also works for the smaller probe, as can be seen in Figure 5.4.

Figure 5.4: The small hand-made probe tracked with Kinect's skeletal tracking.

5.3 Magnetometer performance

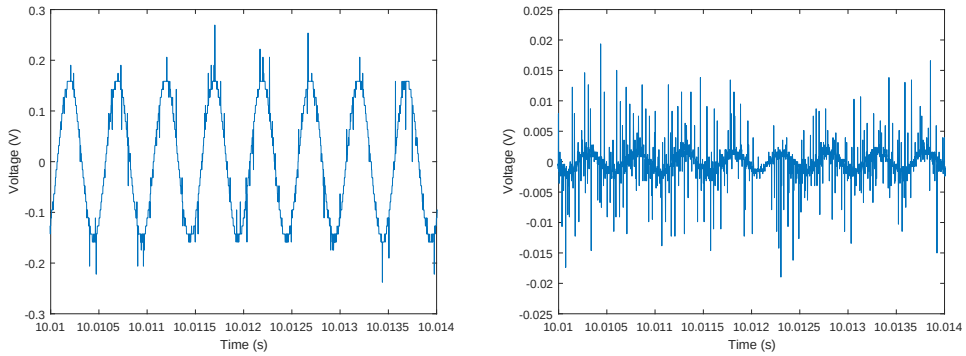

Figure 5.5: Voltage in the x-coil of the a) Narda probe b) STUK's probe. The frequency of the source was 1 kHz.

The signals in Figure 5.5 have been measured from the same 1 kHz magnetic field source using the two magnetic field probes available in this project. The signal of STUK's probe contains much more noise than Narda's signal. This is due to the fact that STUK's probe lacks shielding. Also the amplitude is much smaller in the hand-made probe, due to its smaller size and smaller amount of turns. The induced voltage increases with increasing amount of loops in the coil. The smaller probe is more fit for measuring field distributions from small sources.

5.4 Test measurements

A couple of test measurements were done in order to evaluate the performance of the measurement system. The system was tested by performing measurements using simple coils, a squared coil and a circular coil, as magnetic field sources. The test coils are shown in Figure 5.6. A function generator was used as a power source for the coils. In this way the magnetic field produced by the coils had a known frequency.

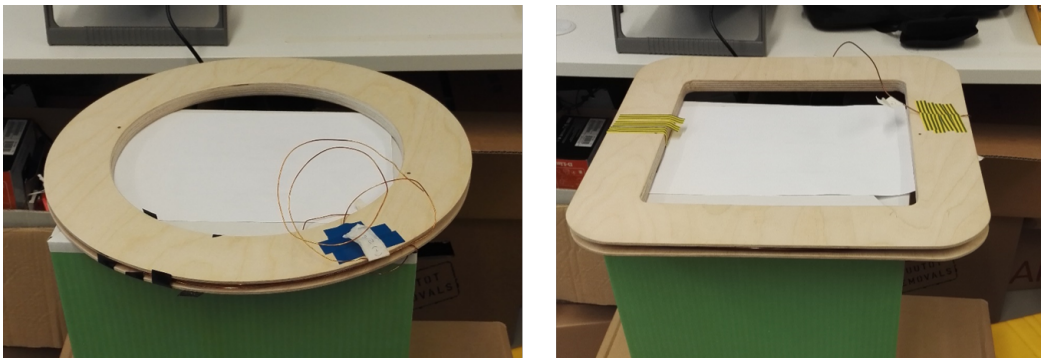

Figure 5.6: Coils used for testing the system. a) Circular coil b) square-shaped coil

5.4.1 Circular coil

The system was first tested with a circular coil with a diameter of 43.3 cm and 236 turns. A 200 mA alternating current with a 1 kHz frequency was fed to the coil. The measurement time was 200 seconds, because the data points needed to cover a large area.

As can be seen from the spectrogram and frequency spectrum in Figure 5.7, the dominant frequency is 1 kHz and noise sources with a frequency of 150 Hz and a weak source of 450 Hz and a DC offset are present. These frequency components appear to have constant strengths throughout the measurement, as can be seen from the spectrogram.

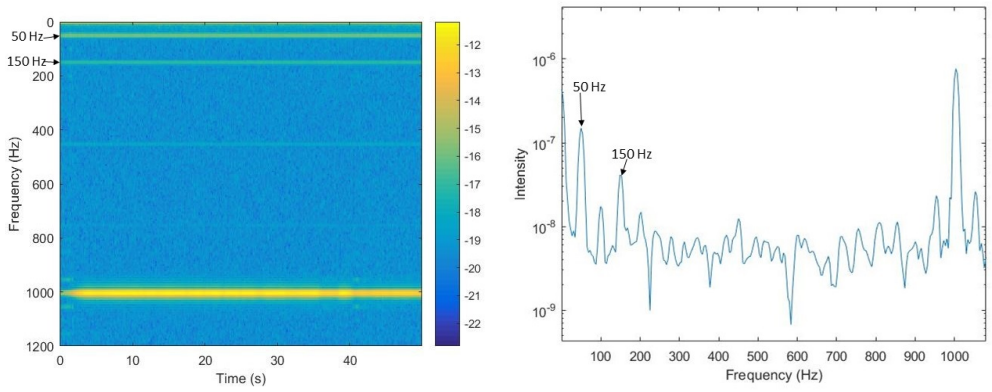

Figure 5.7: Spectrogram and frequency spectrum of the circular test coil with 1 kHz frequency.

The trajectory of the magnetometer probe and the strength of the magnetic field through this trajectory are shown in Figure 5.8. The 50 Hz magnetic field in Figure 5.8 b is noise. As can be seen from Figure 5.8 a, the magnetic field of the coil is strongest above the ring of the coil and reduces with distance to the coil. The maximum field in this case is about 2.8 µT. One strong source for the 50 Hz field was detected to be the function generator used in this measurement. This can be seen in Figure 5.8 b. The function generator is located on the right on the table.

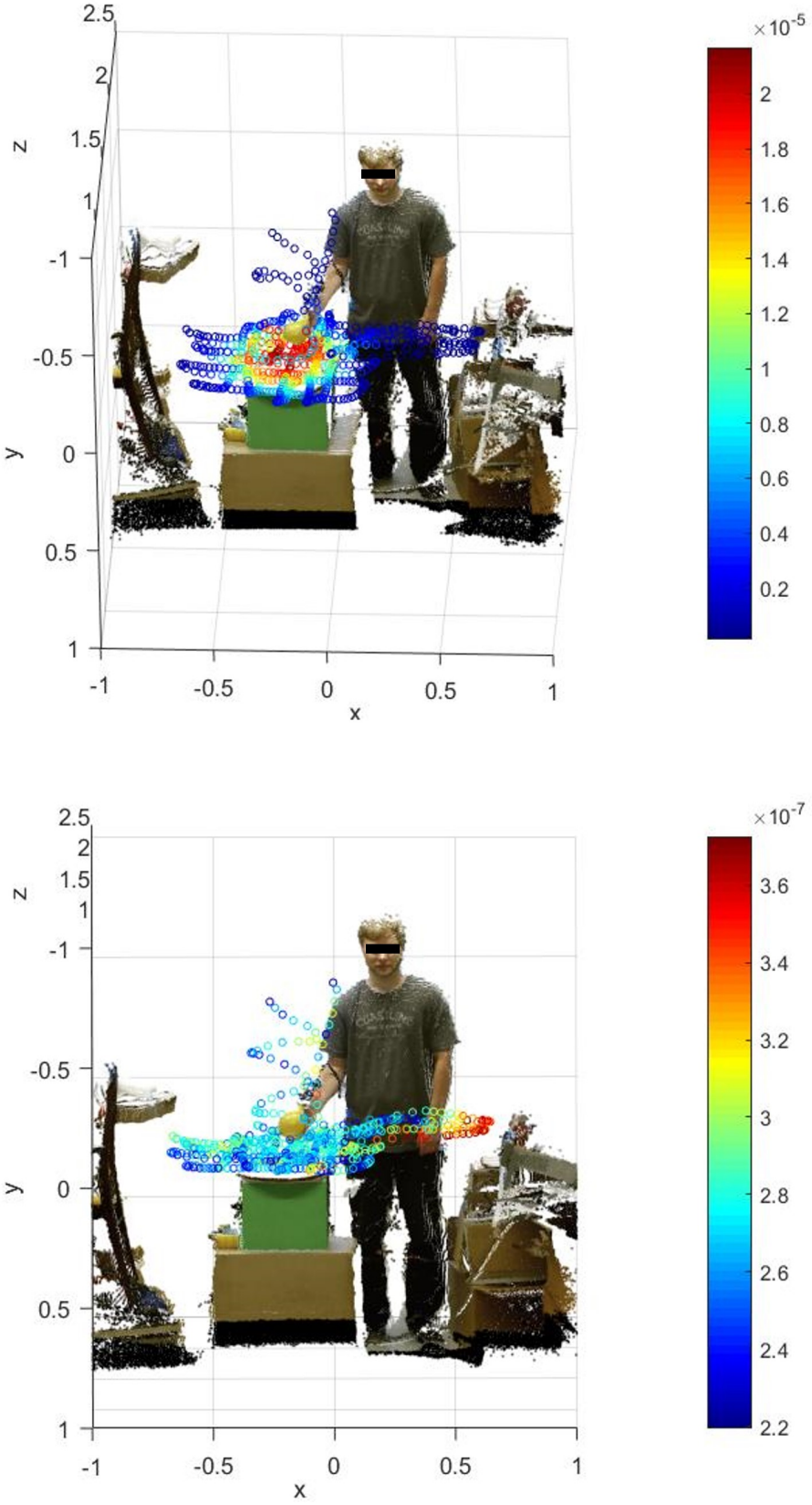

Figure 5.8: Visualization of the trajectory of the probe and the magnetic field in Teslas in the test measurement. Visualization has been created in Kinect point cloud achieved from the measurement scene. a) The strength of the 1 kHz magnetic field. b) The strength of the 50 Hz magnetic field.

5.4.2 Squared coil

A square-shaped coil with 120 turns worked as the second test coil. It has a diameter of 43.7 cm. The frequency was again set to 1 kHz and the magnitude of the current was 200 mA. The measurement was performed with the two available magnetic field probes. Measurement time was 100 seconds.

The spectrum and the spectrogram of the measurement are shown in Figure 5.9. There was less noise present compared to the measurement with the circular coil: only slight 50 Hz noise.

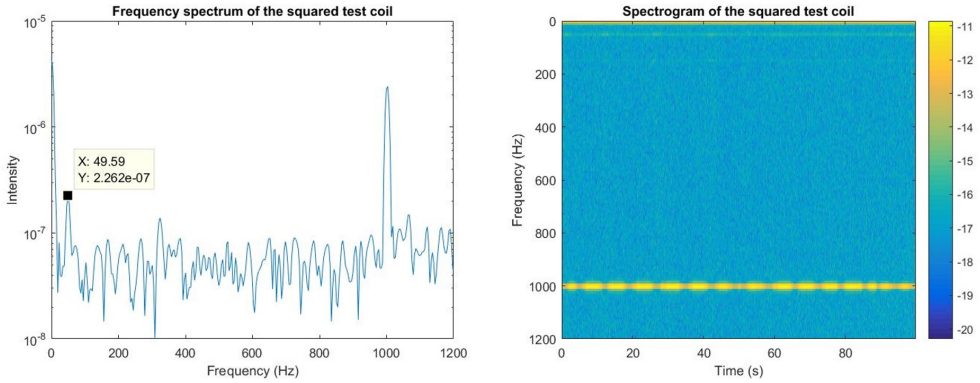

Figure 5.9: The frequency spectrum and the spectrogram of the squared test coil with 1 kHz frequency.

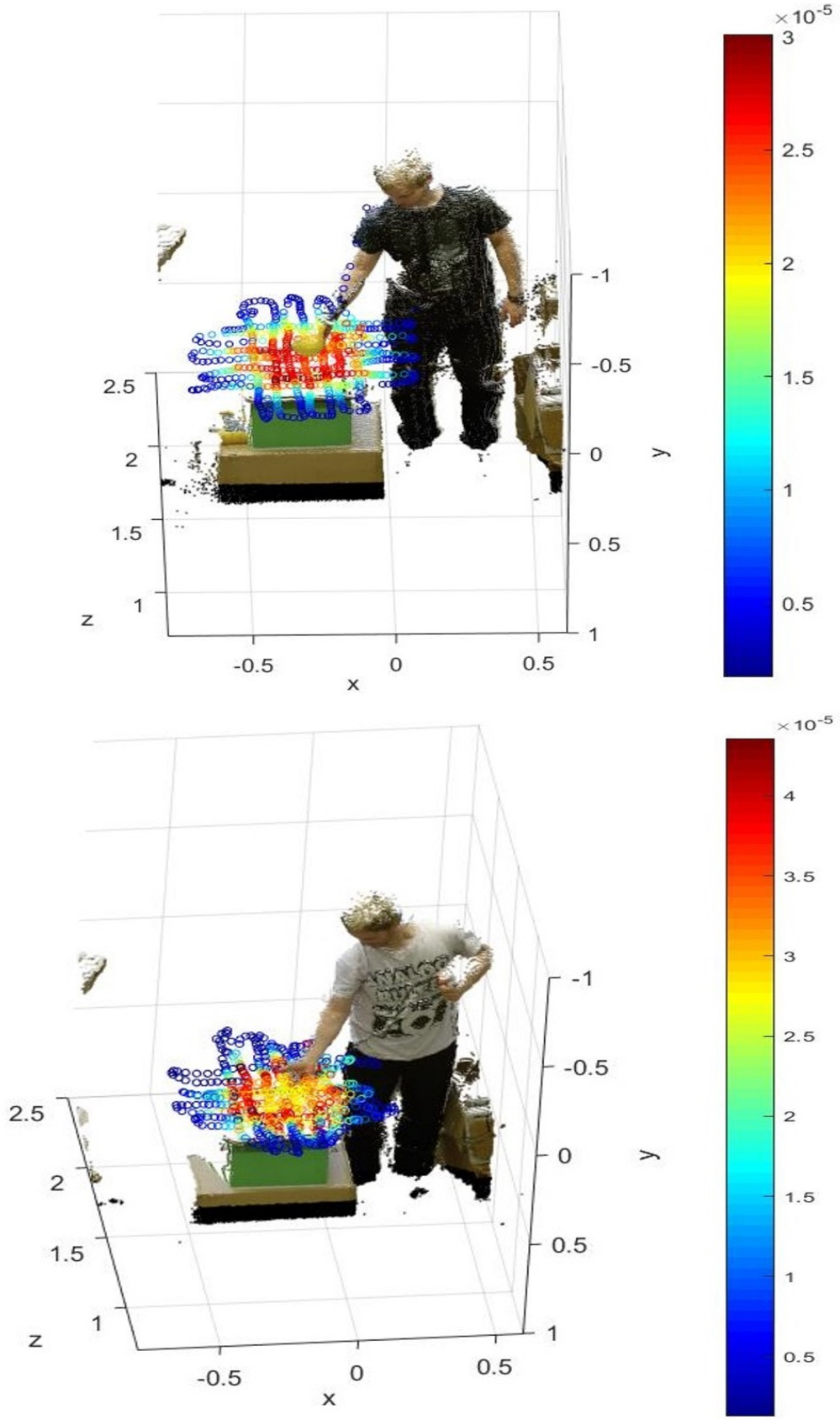

Figure 5.10: Visualization of the trajectory of the probe and the magnetic field of the squared test coil in Teslas, when two different probes have been used. a) Narda ELT-400 b) STUK's hand-made probe

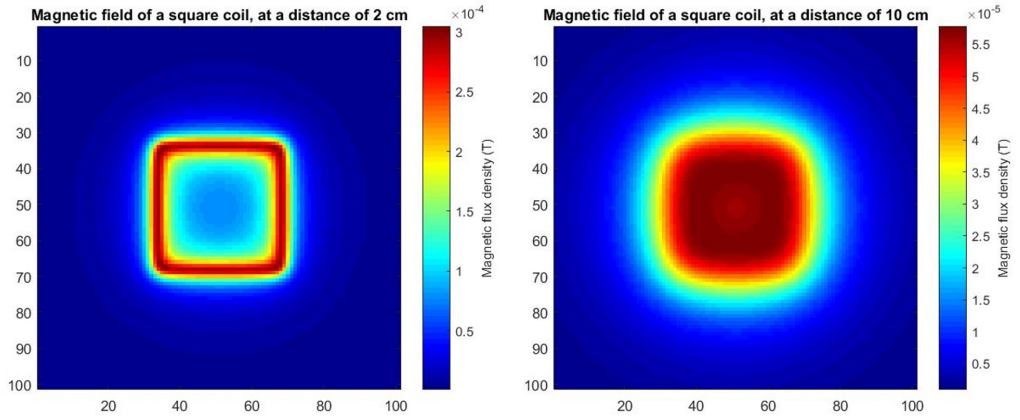

Figure 5.11: Simulated magnetic field distributions of the square test coil at a distance of a) 2 centimeters b) 10 centimeters from the coil surface.

Figure 5.10 shows the magnetic field distribution of a squared coil measured both with Narda's probe and the hand-made probe. In both test measurement coils the field does not reach very far. In these two measurements, the distribution seems to be slightly different as well as the strength of the field. Narda's magnetometer finds the strongest field in the center of the coil, while the smaller probe locates the maximum field above the windings of the coil. The overall strength of the field is stronger according to the hand-made probe. The maximum field strength in the first measurement is about 30 µT and in the latter 43 µT. Possible cause for this difference is the fact that the hand-made probe has a smaller diameter, which allows it to enter closer to the source in the area of stronger fields. This also explains the difference in the distribution, which can be seen by looking at the simulated images of the magnetic field distribution at different distances in Figure 5.11. The maximum field is located right above the windings in the proximity of the coil, but the maximum moves to the center, when the distance increases.

5.4.3 Two coils with adjacent frequencies

The system was tested by setting the two test coils side-by-side and and feeding them with adjacent frequencies. This test demonstrates the ability of the system to separate magnetic fields with different frequencies. The results also give an idea about the frequency resolution of the measurement system. The data was processed using the Hann window instead of flat top, which provided better results. The spectrograms in Figures 5.12 and

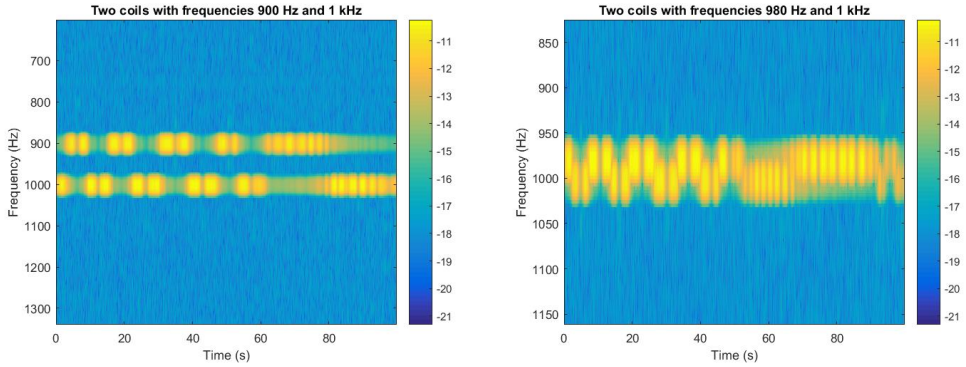

(a) Frequencies 900 Hz and 1 kHz (b) Frequencies 980 Hz and 1 kHz

Figure 5.12: Spectrograms of the setup where the coils have clearly different frequencies

5.13 demonstrate, how the measurement system is capable of distinguishing between the different frequencies quite accurately. The movement of the probe from on top of one coil over the other during the measurement is the reason for the pattern in the spectrograms. The spectral lines of the different frequencies become merged as the frequencies of the test coils approach each other, as can be seen in Figures 5.12b, 5.13a and 5.13b. Frequencies with a

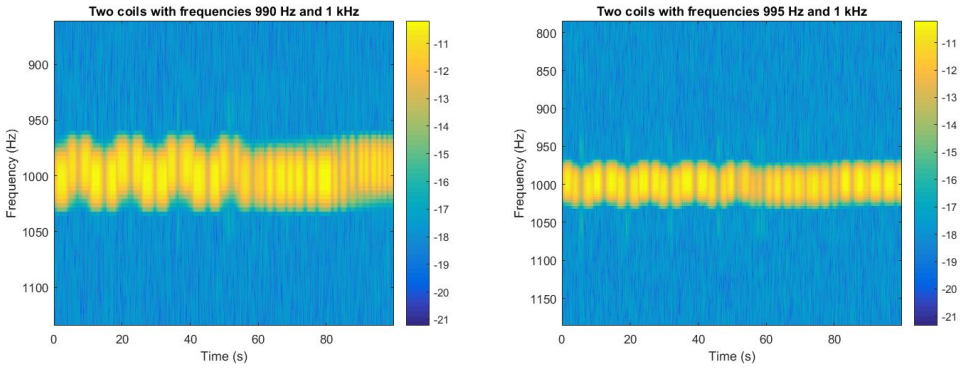

(a) Frequencies 990 Hz and 1 kHz (b) Frequencies 995 Hz and 1 kHz

Figure 5.13: Setup, where the frequencies are barely separable (a) and non-separable (b)

separation of 10 Hz were still barely distinguishable, but when the difference was only 5 Hz the frequencies became indistinguishable. This is illustrated in Figures 5.14 and 5.15. When the frequencies are 990 Hz and 1000 Hz, the circular test coil on the right can be identified to be the source of the lower frequency field. When the frequencies have a mere separation of 5 Hz, the two fields are no longer distinguishable and they both seem to originate from the squared coil on the left. The frequency resolution of this system is therefore 10 Hz. The theoretical frequency resolution depends on the length of the window used in data processing.

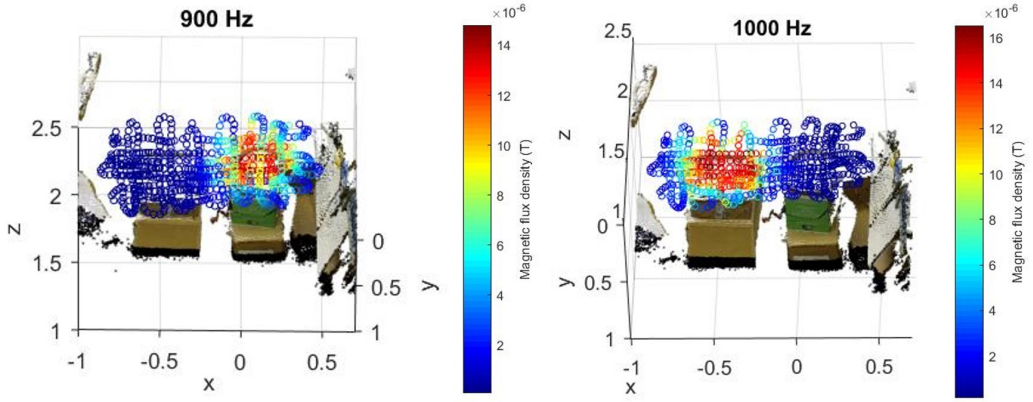

Figure 5.14: Two magnetic fields with frequencies 990 Hz and 1000 Hz are still distinguishable.

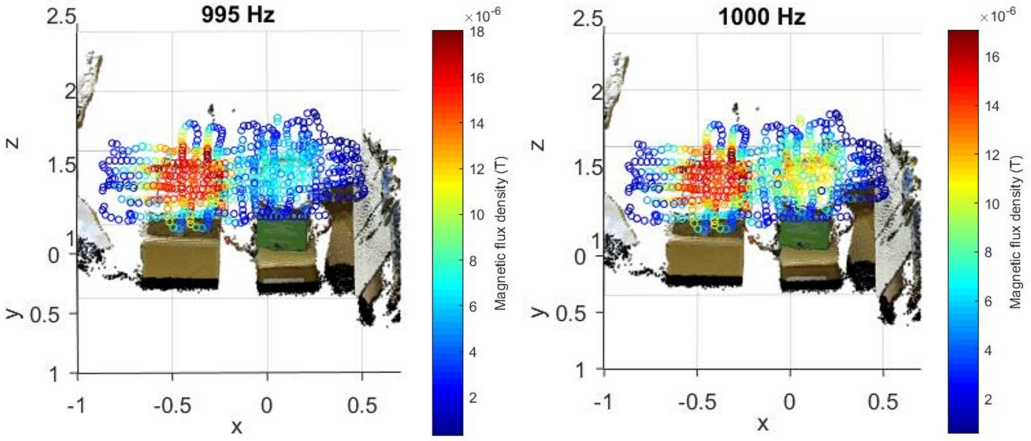

Figure 5.15: Two fields with frequencies 995 Hz and 1000 Hz are no longer distinguishable.

The system was also tested with frequencies close to 100 Hz and 3 kHz. The frequency resolution was the same 10 Hz with frequencies close to 100 Hz. With higher frequencies approaching 3 kHz the frequency resolution was 20 Hz, but the field strengths were smaller compared to lower frequencies, which complicated the separation between them.

5.5 Magnetic field distribution of a vacuum cleaner

The magnetic field distribution of a running vacuum cleaner was measured using a measurement time of 100 seconds. As can be seen from the spectrogram and the frequency spectrum in Figure 5.16, the dominant field has a frequency of 50 Hz. This was expected, due to the fact that the frequency of

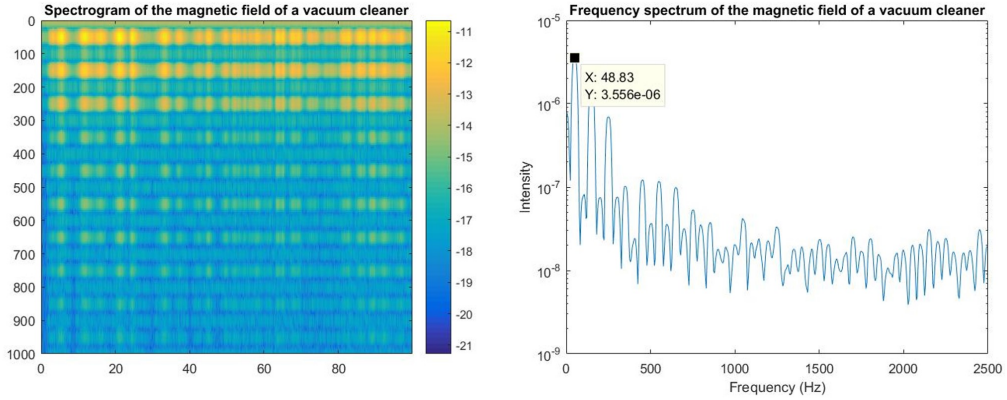

Figure 5.16: Spectrogram and frequency spectrum of vacuum cleaner's magnetic fields

the mains current is 50 Hz. The spectrogram shows that the field is characterized also by harmonic frequencies of the 50 Hz magnetic field, which are the frequencies that appear on the spectrogram in addition to the fundamental frequency with an interval of 100 Hz. The distribution of these harmonic fields is very similar compared to the distribution of the dominant 50 Hz field, but they are weaker, as can be seen in Figure 5.17. All these fields seem to originate from a certain area of the vacuum cleaner, a lower corner, which is presumably the location of the motor. These kind of harmonics are indeed characteristic of an electrical motor (Ellis and Eng, 2001). Similar harmonics appear also in the magnetic fields originating from a hairdryer and a drill.

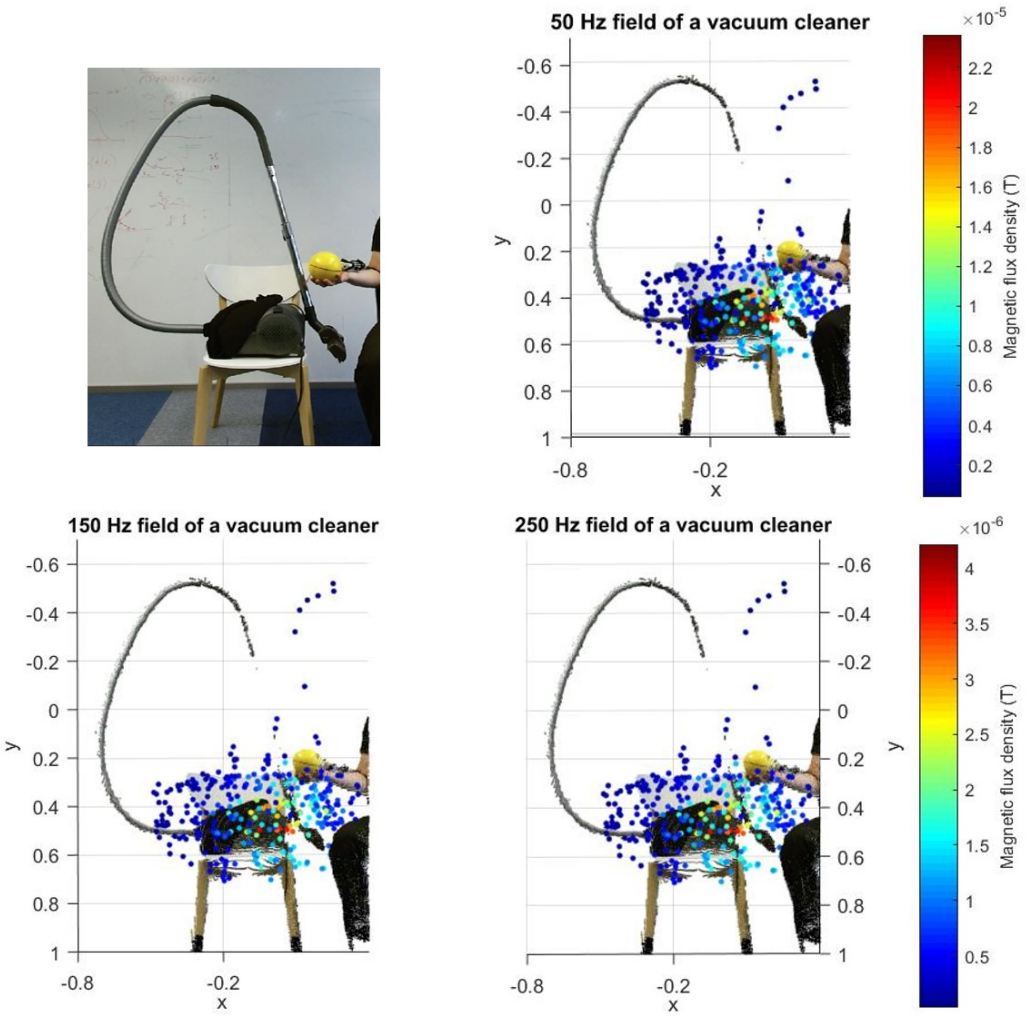

Figure 5.17: Magnetic field distributions of the vacuum cleaner's magnetic field in different frequencies

5.6 The magnetic field of an induction cooker

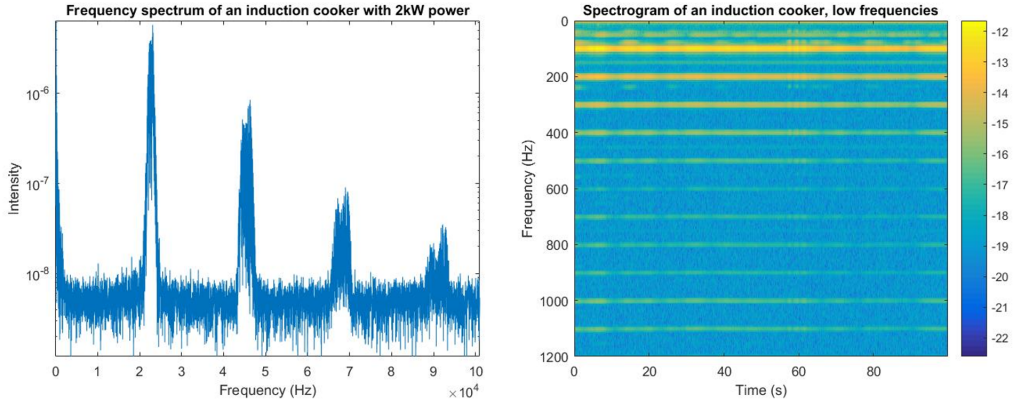

Figure 5.18: Frequency spectrum and spectrogram of an induction cooker with a power of 2 kW

The frequency spectrum and the spectrogram of an induction cooker are presented in Figure 5.18. The highest amplitude is in the frequency of 100 Hz, even though the main frequency of the induction cooker is expected to be around 24 kHz (Wilson, 2006). A peak is also seen in the frequency spectrum in the frequency of 23 kHz, which should be the frequency of the induction. A field with a higher amplitude, however, exists in the 100 Hz frequency. It probably originates from the rectifier, that rectifies the 50 Hz mains current (Wilson, 2006). The magnetic field emission of the induction cooker is characterized with harmonic frequencies of both the 100 Hz and 23 kHz.

The maximum of the 100 Hz magnetic field of the cooker, when running in its full power, was about 21 µT measured with Narda's probe. The 100 Hz field is strongest behind the cooker, which is shown in Figure 5.19 on the right.

The visualization of the strength of the field induced by the induction coil is difficult, due to the width of the frequency peak around the frequency of induction. The 23 kHz field of the induction cooker is modulated with 100 Hz, which can be seen from Figure 5.20. A wide frequency peak is typical of such modulated fields (Nyberg and Jokela, 2006, Chapter 2). The approximations of the total field is calculated, as explained in Section 4.6.2, by summing the amplitudes of adjacent frequencies building up the peak. The resulting magnetic field distribution is shown in Figure 5.21. Because of the summation, the strength of the field appears higher than it actually is.

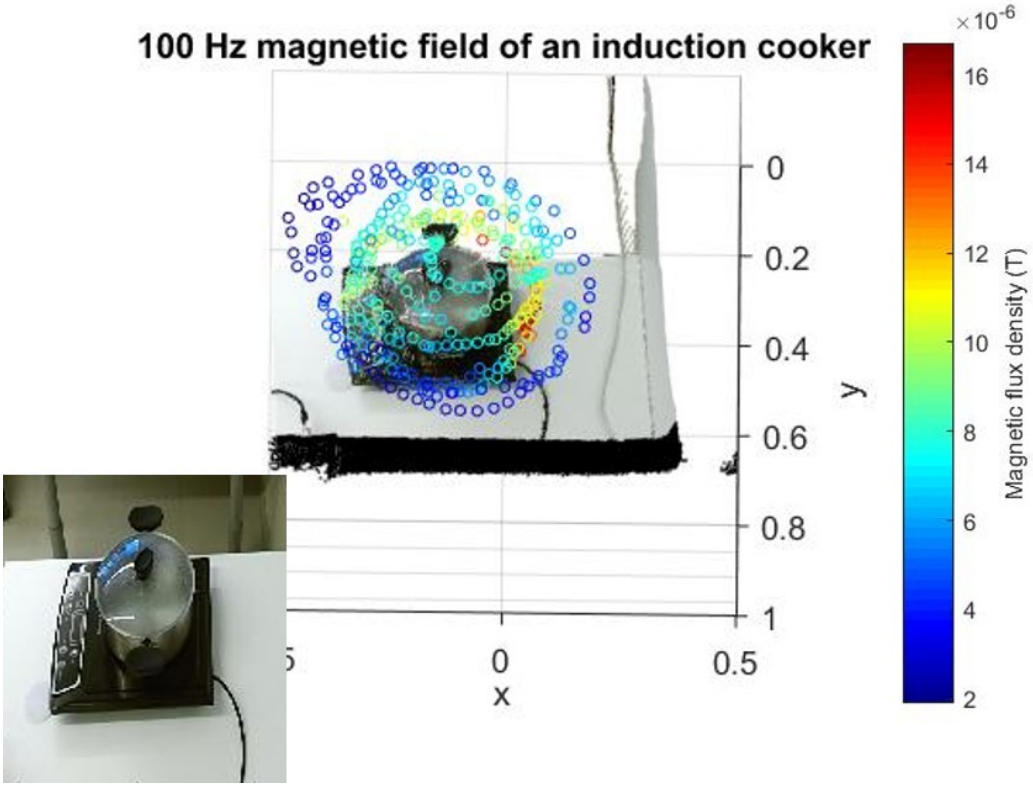

Figure 5.19: Distribution of the 100 Hz magnetic field of an induction cooker running on full power (2000 W)

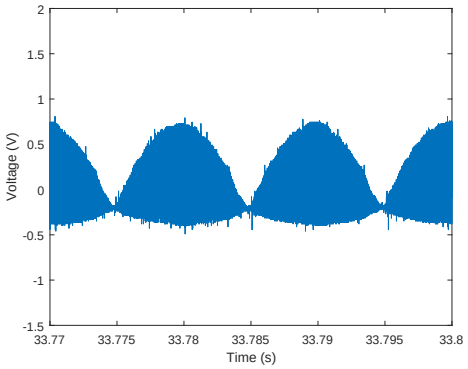

Figure 5.20: The 23 kHz field of the induction cooker is modulated by 100 Hz.

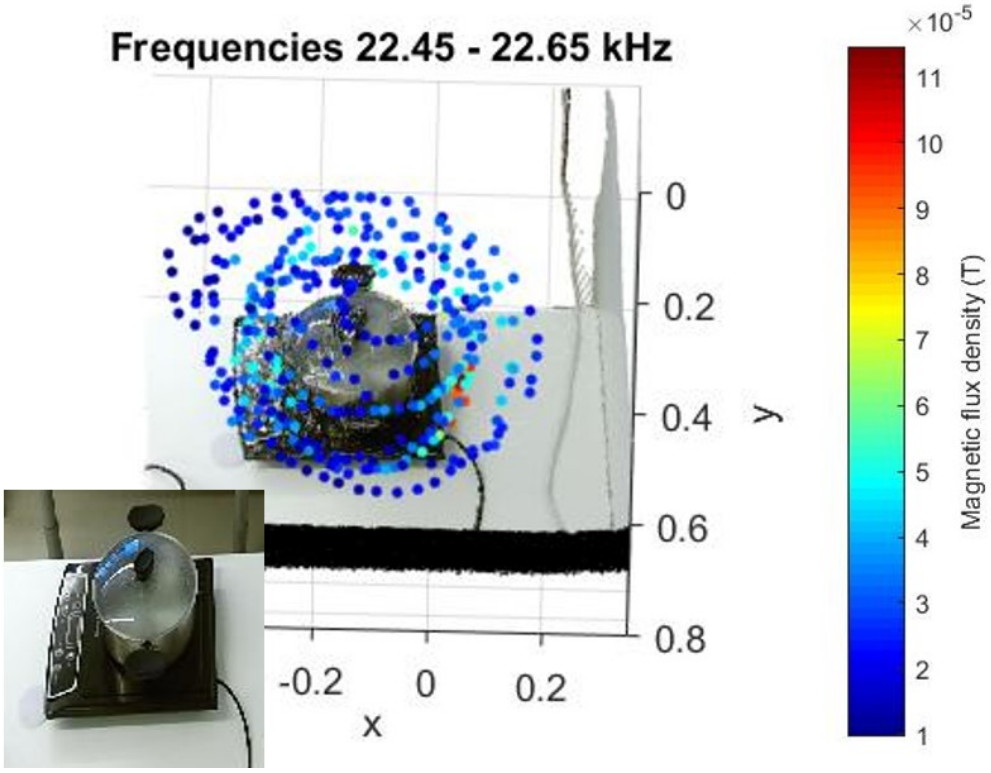

Figure 5.21: Distribution of the induction cooker's field between frequencies 22.45 and 22.65 kHz.

5.7 Magnetic field distribution of an electronic surveillance gate

This particular gate was expected to work in the radio frequency area, meaning frequencies between 3 kHz and 300 GHz. During the measurements, however, 50 Hz appeared to be the dominant frequency with the strongest amplitude. With further examination, the 50 Hz field was found to originate from under the floor because it existed in other spots around the room and not just in the proximity of the gate. The likely sources of this field are cables running below the floor. Figures 5.22 and 5.23 illustrate how the 50 Hz field with similar distribution exists next to the gate and not only in the gate's area. The field is stronger outside the gate, which also indicates that the gate is not the source for the 50 Hz magnetic field.

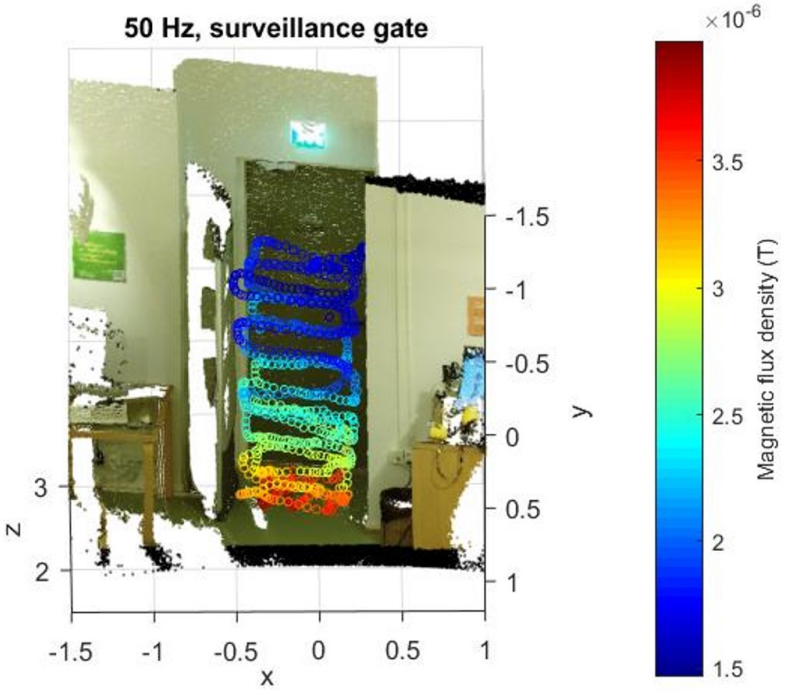

Figure 5.22: Distribution of a 50 Hz magnetic field

Further evaluation of the gate's frequency was performed with a test receiver for radio frequencies, and the frequency of the gate was confirmed to be 13.56 MHz. This is the dominant frequency of radio frequency identification (RFID) library systems similar to this one (Molnar and Wagner, 2004).

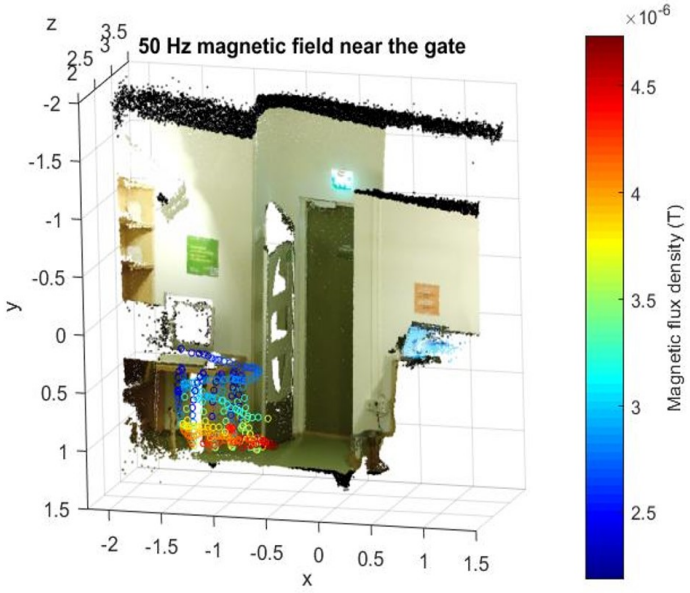

Figure 5.23: Distribution of a 50 Hz magnetic field near the gate

The frequency is outside the frequency range of the magnetic field probes used in this project and in addition to that the sampling rate of the PicoScope's streaming mode is insufficient for measuring frequencies as high as that. The 440 kHz peak in the frequency spectrum measured in real time with the PicoScope in Figure 5.24 is a result of aliasing of the 13.56 MHz frequency because of the insufficient sampling rate (National Instruments, 2016).

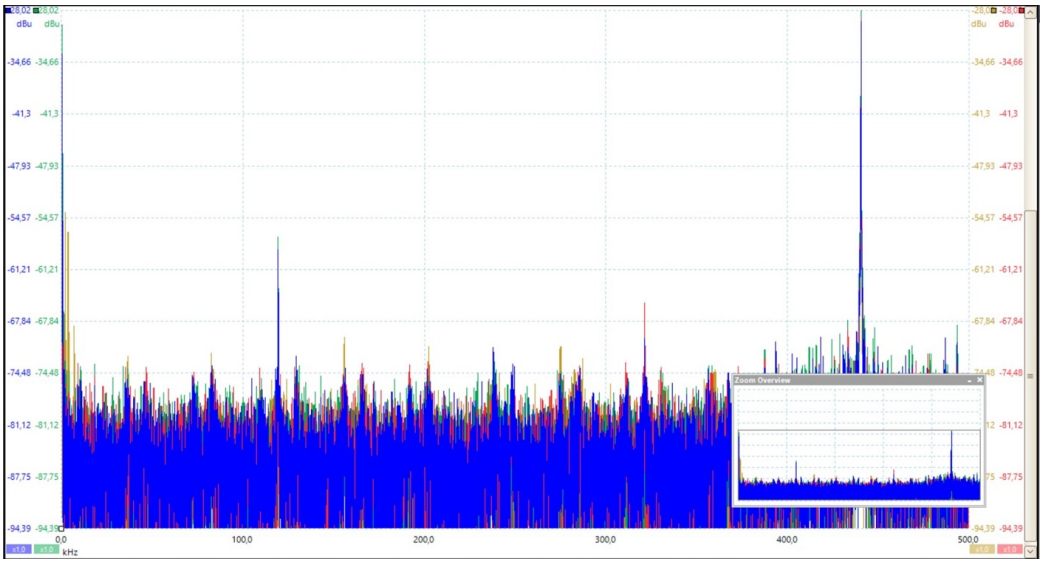

Figure 5.24: Aliased frequency of 13.56 MHz in the frequency spectrum of an electronic surveillance gate.

5.8 Other sources

As expected, the main frequencies of the magnetic fields of a hair dryer and an old drill were both 50 Hz, as can be seen from their spectrograms in Figure 5.25. Both emissions were also characterized with harmonics of the 50 Hz field, which appear because of the electric motors of the devices. The harmonics of the hair dryer appear on the spectrogram with an interval of 50 Hz whereas the harmonics of the drill have a 100 Hz interval. The maximum value of the dominant fields of the dryer and drill are approximately 12 µT and 55 µT, respectively. The visualizations in Figure 5.26 and Figure 5.27 demonstrate that the fields from these devices do not reach very far from their sources.

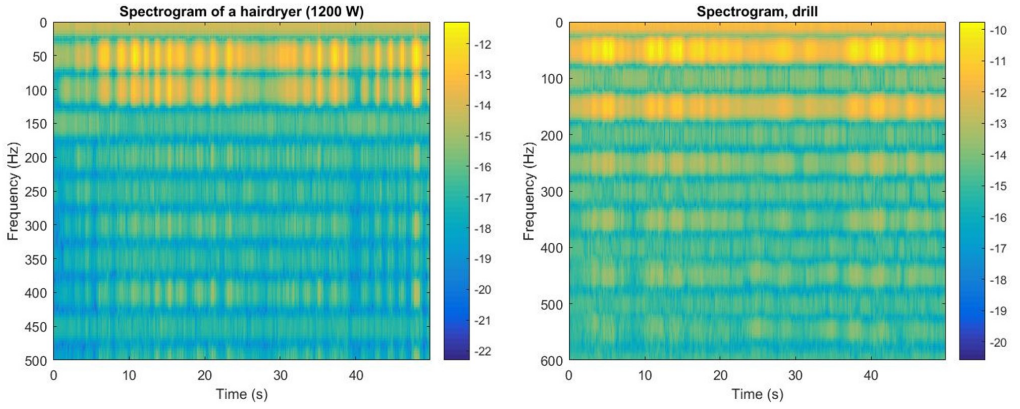

Figure 5.25: Spectrograms of the magnetic fields of a a) hair dryer and a b) drill.

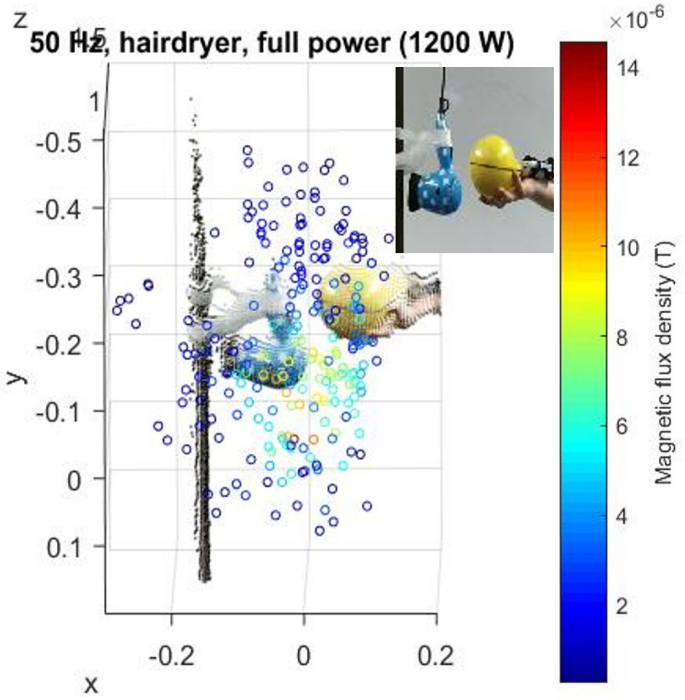

Figure 5.26: Magnetic field distribution of a hairdryer.

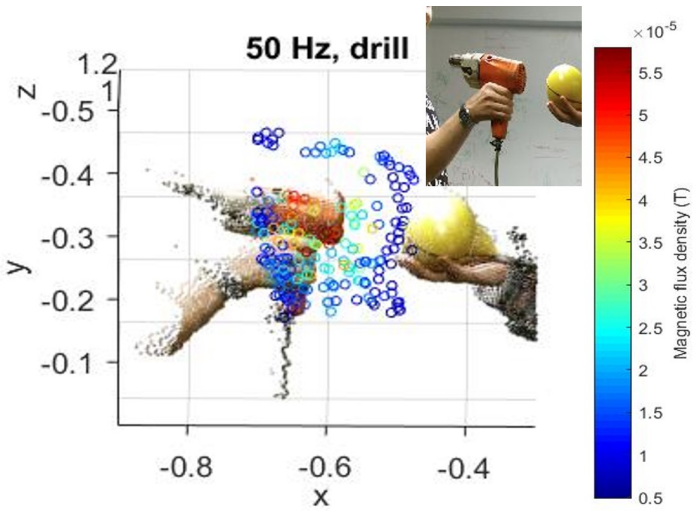

Figure 5.27: Magnetic field distribution of a drill.

5.9 Measuring pulsed magnetic fields

Figure 5.28: A pulsed electronic surveillance gate

Measuring pulsed fields is not what this system excels at with the current settings. The durations of the pulses are usually so short that it renders insufficient time for measuring the spatial distribution of the magnetic field. The strength of the pulse can then be measured only in a single point. In Figure 5.29 is depicted the voltage induced to the x-coil of Narda's probe while measuring the magnetic field distribution of an electronic surveillance gate. The gate (Figure 5.28) uses pulsed magnetic field in the detection of stolen items. As can be seen from Figure 5.29, the pulse is very short with a duration of only about 20 milliseconds. Otherwise only the background EMF are present. The Kinect has a frame rate of 0.16 seconds, which means that achieving one frame and the associated position data takes 160 ms. During the pulse there is not enough time for collecting the position of the probe.

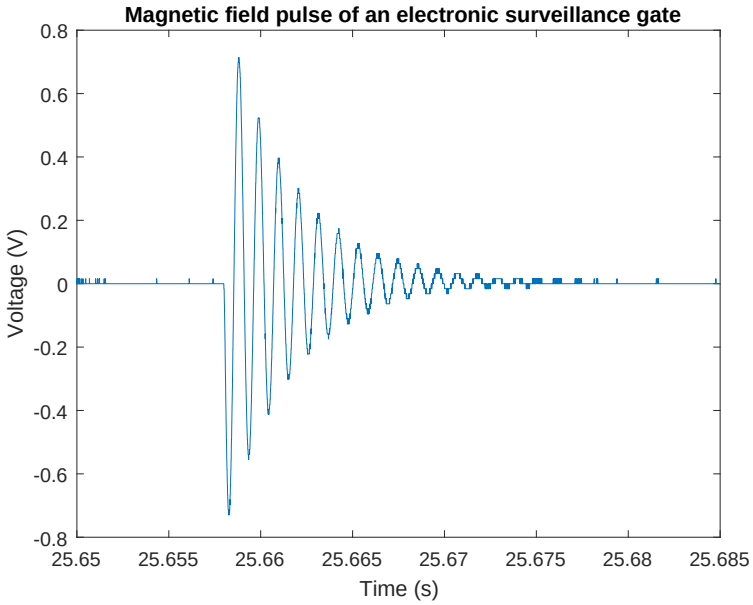

Figure 5.29: Voltage in the x-coil of ELT-400 induced by a pulsed magnetic field of an electronic surveillance gate.

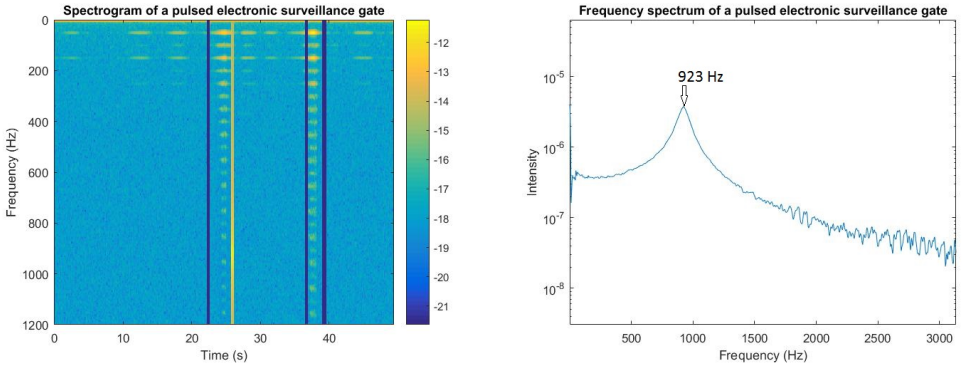

(a) Spectrogram of a pulsed surveillance gate

(b) Frequency spectrum of the pulsed magnetic field of the gate

Figure 5.30: Spectrogram of a pulsed surveillance gate and the frequency spectrum of the pulse

The pulse was so strong that it caused the magnetometer to become overloaded, when it was run in its 320 high -mode. This indicates that the magnetic flux density of the pulse was at least 320 µT. Overload causes the measurement of the magnetic field to be interrupted, which appears in the spectrogram Figure 5.30a as dark blue lines with value "NaN". The frequency distribution of the pulse is shown in Figure 5.30b, where the dominant frequency of the peak is 923 Hz.

The pulsed magnetic field of a wireless power transfer device had a longer duration of four seconds. The frequency of the pulse was around 240 kHz and the maximum strength of the field during the pulse was 400 µT. The maximum field emerged in front of the device. The duration of the pulse was sufficiently long for the calculation of its frequency spectrum and the strength of the field emission in the device's main frequency. The pulse strength and the spectrum are shown in Figure 5.31 a and b, respectively. During a four second pulse, the Kinect collects around 30 positions of the

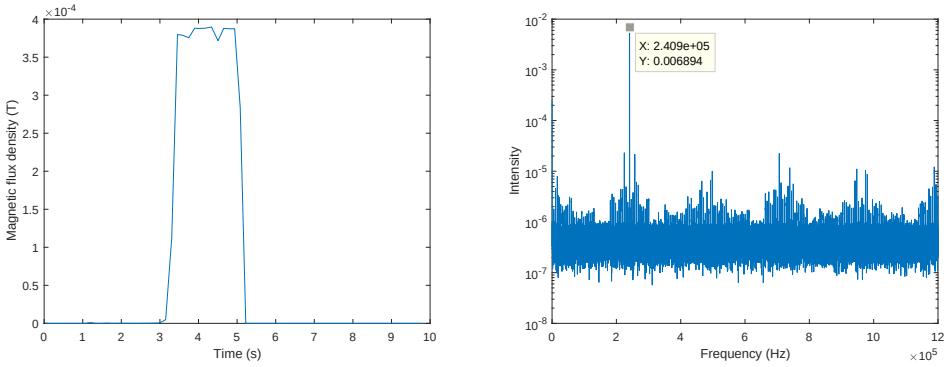

Figure 5.31: a) The strength of the pulsed magnetic field of a wireless power transfer device and its b) spectrum.

probe. Nevertheless, due to the slowness of the user's hand, this duration is too short for acquiring an informative spatial distribution of the pulsed field.

Chapter 6

Discussion

A functioning system was created and its performance was tested in ways shown in Chapter 5. The performance of the system, the dangerousness of the measured fields and future prospects are discussed in this chapter.

6.1 The performance of the system

The approach of tracking the probe by means of computer vision was the initial method in this project. Of various methods that were tested, the fitting of a sphere to a point cloud appeared to be the best. An advantage of this method compared to the skeletal tracking is that it does not require the presence of the user in the measurement scene. This enables the use of this system for the measurement of electric fields as well. However, this method is dependent on the properties, more precisely on the color and shape of the probe and needs to be modified in the case of using another probe. This method is not suitable for tracking the smaller magnetic field probe made by STUK, since it does not have a color as distinctive as the color of Narda's probe or a clear shape that can be used in the point cloud shape fitting.

The reliability of the sphere fitting method is not very high due to the variety of the probe's color because of occlusion or different lighting circumstances. Sometimes the color of the wall is too close to the average color of the probe or other yellow objects exist in the background, which disturb the functionality of this method. Also the poor quality of the point cloud due to missing information worsens the outcome.

The body tracking ability of the Kinect sensor was chosen for the positioning in this project. One clear advantage of using the body tracking for acquiring the position of the probe is that it is not dependent on the properties of the probe we are using. Because the location tracking is based on

tracking the hand, it works with other kinds of probes as well. It presumably works even better with a probe of smaller size that can be fit into the users hand. The tracking was successful with both probes that were used in this project. With the current probes, however, failures in tracking occurred sometimes, especially due to arm extension during measurements.

Another advantage of the Kinect is that the measurement results can be quite nicely visualized in 3D in a point cloud achieved from the measurement scene.

A disadvantage of this system is that a full 3D-distribution can not be easily achieved, because the object of interest is blocking the sight for the points behind it.

The current frequency range of the system is 1 Hz - 400 kHz if Narda's probe is used as the magnetometer. The range can be extended by using a magnetometer that can measure fields with higher frequencies. PicoScope's maximum sampling rate sets the maximum frequency of magnetic fields to 1.2 MHz. This is with a measurement duration of only 10 seconds.

The frequency resolution of the system was found to be around 10 Hz, with some dependence on the frequencies. This means that the system can quite accurately separate the frequency components of a magnetic field from each other.

6.2 Concerning the health effects

In general, the magnetic flux densities of the vacuum cleaner, induction cooker, hair dryer or the drill measured in this project did not exceed the safety limits set by EU. The highest magnetic flux density, about 55 µT, appeared in the magnetic field of the drill. This is far from EU's action level, which in the case of magnetic field with a 50 Hz frequency is 1 mT. What is also true for the fields measured in this project is that they did not spread very far from their sources. The body parts most likely to be exposed to magnetic fields are the hands, when holding a drill or cooking with an induction cooker.

6.3 Future prospects

The system still lacks the processing of the location data produced by the Kinect. During the tracking of the probe with Kinect's skeletal tracking, occasional flaws of tracking occur in the form of 'jumping'. Jumping refers to the Kinect losing track of the right hand, or in this case the probe, which can

be seen as the right hand joint in the drawn skeleton jumping to a completely false location. These falsely tracked data points should be excluded from the data using, for example, filtering. The distance measurement of time-of-flight cameras like Kinect is affected by a few noise and error sources. Averaging the measured distances is one fundamental way of reducing noise. (Dal Mutto *et al*, 2012) In any case, the overall accuracy of tracking the probe with Kinect needs to be more precisely assessed.

The orientation of the magnetic field probe can be measured at every time point. The axes of the accelerometer and the gyroscope have already been matched to the real-world axes by choosing a correct starting position for the measurements, as explained in Section 4.4. What is yet to be done, is the synchronization of the probe's measurement axes with the axes of the gyroscope and the accelerometer. Only then the actual direction of the magnetic field at every point can be evaluated. In the case of Narda's probe, this requires utilizing the information given in the operation manual about the orientation of the coils relative to the shaft of the probe.

The system is currently capable of measuring only magnetic fields. It is possible to expand the system in the measurement of electric fields originating from electrical appliances as well. This, however, requires an approach different to the current approach, since the electric fields can not be measured in an environment, where a human is present. The electric field would be distorted by the human and therefore Kinect's body tracking is not suitable for this purpose. The measurement of electric field distributions requires an electric field probe and a way to track the probe's location. A suitable method would be an image processing method for locating the probe in Kinect's images and thus acquiring its three-dimensional location.

The simulation of the induced electric fields by the measured fields is rendered to a later continuation of this project. The calculations require interpolation between data points of the measured magnetic fields, three-dimensional reconstruction of the field and construction of the vector potential (Madsen *et al*, 2015).

This system is a prototype of a hybrid positioning and magnetic field measurement system. The overall appearance and usability of the system needs some improvement, for example enhancing the user interface and automation of saving and processing the data. Currently all data is automatically collected but the processing has to be done by hand. In the future the system should be fully automated, making it more easy-to-use.

Chapter 7

Conclusions

A functioning hybrid positioning and magnetic field measurement system was created in this thesis project. The system measures the magnetic field and simultaneously tracks the position and orientation of the magnetometer. The system utilizes the Kinect sensor for the position tracking and iPhone's built-in accelerometer and gyroscope for the evaluation of the orientation. The magnetic flux density is measured with an induction coil sensor.

Kinect sensor's skeletal tracking ability was utilized in this project: it works well for the tracking of the magnetic field probe. With the current composition the system can be used for the measurement of magnetic fields with frequencies ranging from 1 Hz to 400 kHz. The measurement are performed with freehand scanning and they produce three-dimensional spatial distributions rather rapidly as a result. Depending on the desired complexity of the measurement trajectory, a measurement can be performed in 20 to 200 seconds. Increasing user experience enhances the outcome of the results.

More precise processing of the orientation data is needed for it to become applicable to creating a three-dimensional reconstruction. The location data also needs to be processed in order to exclude errors and make the data more reliable.

The measurement system can provide further knowledge concerning magnetic fields originating from a variety of sources by allowing the visualization of the fields around their sources. The system helps to estimate, how far from their sources the magnetic fields reach, and therefore aids in the protection of people against health effects related to time-varying magnetic fields. The information provided by this system about magnetic field distribution can be of use in product development as well, when determining whether the field of the product meets the requirements related to human exposure or performance. The measurement system created in this project could be useful for the development of wireless power transfer technologies that are based on

resonance between two coils, which means that both the distribution and frequency of the magnetic field have to be carefully adjusted (Kurs *et al*, 2007). The magnetic fields of wireless power transfer systems are also significant in terms of exposure limit values, necessitating detailed assessment of human exposure (Laakso and Hirata, 2012, 2013).

Bibliography

Bi Z, Kan T, Mi C C, Zhang Y, Zhao Z and Keoleian G A 2016 A review of wireless power transfer for electric vehicles: Prospects to enhance sustainable mobility *Applied Energy* **179** 413–425

Dal Mutto C, Zanuttigh P and Cortelazzo G M 2012 Time-of-Flight Cameras and Microsoft Kinect pp. 107–108

Dempsey M F, Condon B and Hadley D M 2002 MRI safety review *Seminars in Ultrasound CT and MRI* **23**(5) 392–401

Ellis R and Eng P 2001 Power System Harmonics - A Reference Guide to Causes, Effects and Corrective Measures *An Allen-Brandley Series of Issues and Answers* pp. 1–14

EU 2013 Euroopan parlamentin ja neuvoston direktiivi 2013/35/EU, ,

Fleder M, Pillai S, Scott J and Csail M I T 2011 3D Object Tracking Using the Kinect pp. 1–8

Han J, Shao L, Xu D and Shotton J 2015 Talent management: Progress and prospects *Human Resource Management Review* **25**(3) 233–235

He H, Maheshwari P, Member S and Pommerenke D J 2016 The Development of an EM-Field Probing System for Manual Near-Field Scanning **58**(2) 356–363

He H, Maheshwari P, Radchenko A and Pommerenke D 2013 EM radiation estimation using an automatic probe position recording system coupled to hand scanning *IEEE International Symposium on Electromagnetic Compatibility* pp. 348–353

Heinzel G, Rüdiger a, Schilling R and Hannover T 2002 Spectrum and spectral density estimation by the Discrete Fourier transform (DFT), including a comprehensive list of window functions and some new flat-top *Max Plank Institute* pp. 1–84

ICNIRP 2010 ICNIRP guidelines for limiting exposure to time-varying electric and magnetic fields (1 Hz- 100 kHz) *Health physics* **99**(6) 818–836

IEC 2005'IEC 62233 : 2005 Measurement methods for electromagnetic fields of household appliances and similar apparatus with regard to human exposure'

IEEE 2002'IEEE Standard for Safety Levels with Respect to Human Exposure to Electromagnetic Fields, 0 - 3 kHz'

IEEE 2010'IEEE Recommended practice for measurements and computations of electric, magnetic and electromagnetic fields with respect to human exposure to such field, 0 Hz to 100 kHz'

Ilvonen S and Sarvas J 2007 Magnetic-field-induced ELF currents in a human body by the use of a GSM phone *IEEE Transactions on Electromagnetic Compatibility* **49**(2) 294–301

Ishida K, Fujioka T, Endo T, Hosokawa R, Fujisaki T, Yoshino R and Hirose M 2016 Evaluation of Electromagnetic Fields in a Hospital for Safe Use of Electronic Medical Equipment *Journal of Medical Systems* **40**(3) 1–11

Kännälä S, Toivo T, Alanko T and Jokela K 2009 Occupational exposure measurements of static and pulsed gradient magnetic fields in the vicinity of MRI scanners. *Physics in medicine and biology* **54**(7) 2243–2257

Kos B, Valič B, Miklavčič D, Kotnik T and Gajšek P 2011 Pre- and post-natal exposure of children to EMF generated by domestic induction cookers. *Physics in medicine and biology* **56**(19) 6149–60

Kurs A, Karalis A, Robert M, Joannopoulos J D, Fisher P and Soljacic M 2007 Wireless power transfer via strongly coupled magnetic resonances *Science* **317**(5834) 83–86

Laakso I and Hirata A 2012 Fast multigrid-based computation of the induced electric field for transcranial magnetic stimulation *Physics in medicine and biology* **57** 7753–7765

Laakso I and Hirata A 2013 Evaluation of the induced electric field *Physics in medicine and biology* **58** 7583–7593

Laakso I, Shimamoto T, Hirata A and Feliziani M 2015 Quasistatic approximation for exposure assessment of wireless power transfer *IEICE Transactions on Communications* **E98B**(7) 1156–1163

Lachat E and Macher H 2015 FIRST EXPERIENCES WITH KINECT V2 SENSOR FOR CLOSE RANGE 3D MODELLING *International archives of photogrammetry and remote sensing* **40**(5) 93

Laukkanen M 2015 Performance Evaluation of Time-of-Flight Depth Cameras

Lenz J and Edelstein S 2006 Magnetic sensors and their applications *IEEE Sensors Journal* **6**(3) 631–649

Lenz J E 1990 A Review of Magnetic Sensors *Proceedings of the IEEE* **78**(6) 973–989

Luinge H J and Veltink P H 2005 Measuring orientation of human body segments using miniature gyroscopes and accelerometers *Medical and Biological Engineering and Computing* **43**(2) 273–282

Lun R and Zhao W 2015 A Survey of Applications and Human Motion Recognition with Microsoft Kinect *International Journal of Pattern Recognition and Artificial Intelligence* (January) 49

Macintyre S a 1999 Magnetic field measurement *CRC Press LLC* pp. 16–18

Madsen K H, Ewald L, Siebner H R and Thielscher A 2015 Transcranial magnetic stimulation: An automated procedure to obtain coil-specific models for field calculations *Brain Stimulation* **8**(6) 1205–1208

Molnar D and Wagner D 2004*in* 'Proceedings of the 11th ACM conference on Computer and communications security CCS 04'number Augustp. 210
URL: *http://portal.acm.org/citation.cfm?doid=1030083.1030112*

Narda 2011 ELT-400 Exposure Level Tester: Operating manual (ELT-400 Exposure Level Tester: Operating manual: 08/11.09, edn)

National Instruments 2016'Aliasing and Sampling at Frequencies Above the Nyquist Frequency'
URL: *http://www.ni.com/white-paper/3000/en/*

Niu X, Zhang Q, Li Y, Cheng Y and Shi C 2012 Using inertial sensors of iPhone 4 for car navigation *Record - IEEE PLANS, Position Location and Navigation Symposium* pp. 555–561

Nyberg H and Jokela K 2006 Säteily- ja ydinturvallisuus 6: Sähkömagneettiset kentät (Säteily- ja ydinturvallisuus 6: Sähkömagneettiset kentät: Säteilyturvakeskus)

Robbes D 2006 Highly sensitive magnetometers-a review *Sensors and Actuators, A: Physical* **129**(1-2 SPEC. ISS.) 86–93

Sarkka S, Tolvanen V, Kannala J and Rahtu E 2015 Adaptive Kalman filtering and smoothing for gravitation tracking in mobile systems *2015 International Conference on Indoor Positioning and Indoor Navigation (IPIN)* (October) 1–7

Sato K, Kawata H, Kashimura Y and Kamimura Y 2012*in* 'IEEE International Symposium on Electromagnetic Compatibility'

Sato K, Takasu Y and Kamimura Y 2014 A study of a measuring method for EMF distributions using the Kinect sensor *Electromagnetic Compatibility (EMC Europe), 2014 International Symposium on* pp. 1214–1217

Shotton J, Sharp T, Kipman A, Fitzgibbon A, Finocchio M, Blake A, Cook M and Moore R 2013 Real-time Human Pose Recognition in Parts from Single Depth Images *Commun. ACM* **56**(1) 116–124

Starlino 2009'A guide to using IMU'
URL: *http://www.starlino.com/imu_guide.html*

Terven J R and Córdova-Esparza D M 2016 Kin2. A Kinect 2 Toolbox for MATLAB *Science of Computer Programming* (May)

Tong Z Y, Dong Z Y and Tong M M 2016 Analysis of magnetic field generated by overhead cables *Measurement* **89** 166–170

Tumanski S 2007 Induction coil sensors - a review *Measurement Science and Technology* **18**(3) R31–R46

Tumanski S 2011 Handbook of Magnetic Measurements (Handbook of Magnetic Measurements: CRC Press)

Waffenschmidt E 2011*in* 'IEEE International Telecommunications Energy Conference (INTELEC)'pp. 1–9
URL: *http://ieeexplore.ieee.org/xpl/articleDetails.jsp?tp=&arnumber=6099840&searchWithin=p_First_Names:Eberhard&searchWithin=p*

WHO 2007 Environmental Health Criteria 238 EXTREMELY LOW FREQUENCY FIELDS *World Health Organization* (35) 543

Wilson L R 2006'Operation of a 2 kW induction cooker'
URL: *http://imajeenyus.com/electronics/20060908_induction_cooker/index.shtml*

Woodman O J 2007 An introduction to inertial navigation, ,
URL: *http://www.ncbi.nlm.nih.gov/pubmed/19863683*

Xu X and McGorry R W 2015 The validity of the first and second generation Microsoft Kinect for identifying joint center locations during static postures *Applied Ergonomics* **49** 47–54

Yang L, Zhang L, Dong H, Alelaiwi A and Saddik A 2015 Evaluating and improving the depth accuracy of Kinect for Windows v2 *IEEE Sensors Journal* **15**(8) 4275–4285

Young H D and Freedman R A 2012 University Physics with Modern Physics (University Physics with Modern Physics: 13th edn)

Appendix A

Collection of position data

Collection of body tracking data with Kinect:

```
%% BODYDEMO Illustrates how to use the Kin2 object to
   get and draw the
% Skeleton data

% Original code by:
% Juan R. Terven, jrterven@hotmail.com
% Diana M. Cordova, diana_mce@hotmail.com

% Edited by:
% Laura Jukola

% Citation:
% J. R. Terven, D. M. Cordova, "A Kinect 2 Toolbox for
   MATLAB",
% https://github.com/jrterven/Kin2, 2016.

% Initialize the arduino microcontroller
 s = serial('COM4');
 fopen(s);

addpath C:\Python27
addpath('Mex');
%clear all
close all
orient_tw = [];
time_f = [];
%time_p =[];
```

```
%t = 0;
clear 'hand_r'
clear 'hand_l'
clear 'n'

% Create Kinect 2 object and initialize it
% Available sources: 'color', 'depth', 'infrared', '
    body_index', 'body',
% 'face' and 'HDface'
k2 = Kin2('color','depth','body');
% Collect frames
depth_frames = struct([]);
color_frames = struct([]);

% images sizes
d_width = 512; d_height = 424; outOfRange = 4000;
c_width = 1920; c_height = 1080;
%tic % Here the time starts: therefore the time of the
    first data point might not be 0, because time was
    running before the first body was tracked

% Color image is to big, let's scale it down
COL_SCALE = 1.0;

% Create matrices for the images
depth = zeros(d_height,d_width,'uint16'); % Buffers
color = zeros(c_height*COL_SCALE,c_width*COL_SCALE,3,'
    uint8');

% depth stream figure
d.h = figure;
d.ax = axes;
d.im = imshow(zeros(d_height,d_width,'uint8'));
%hold on;

title('Depth Source (press q to exit)')
set(gcf,'keypress','k=get(gcf,''currentchar'');'); %
    listen keypress

% color stream figure
c.h = figure;
```

```
c.ax = axes;
c.im = imshow(color,[]);
title('Color Source (press q to exit)');
set(gcf,'keypress','k=get(gcf,''currentchar'');'); % listen keypress
%hold on
hetki = cell([],111);
acc = [];
gyr = [];
mag = [];
%pos_sum = 0; orient_sum = 0;
% Loop until pressing 'q' on any figure
k=[];
n=1;
disp('Press q on any figure to exit')
while true
    %tic
    % Get frames from Kinect and save them on underlying buffer
    validData = k2.updateData;

    % Before processing the data, we need to make sure that a valid
    % frame was acquired.
    if validData
        % Copy data to Matlab matrices
        depth = k2.getDepth;
        color = k2.getColor;

        % update depth figure
        depth8u = uint8(depth*(255/outOfRange));
        depth8uc3 = repmat(depth8u,[1 1 3]);
        d.im = imshow(depth8uc3, 'Parent', d.ax);

        %set(d.im,'CData',depth8uc3);

        % update color figure
        color = imresize(color,COL_SCALE);
        c.im = imshow(color, 'Parent', c.ax);

        %set(c.im,'CData',color);
```

```
% Get 3D bodies joints
% Input parameter can be 'Quat' or 'Euler' for
    the joints
% orientations.
% getBodies returns a structure array.
% The structure array (bodies) contains 6
    bodies at most
% Each body has:
% -Position: 3x25 matrix containing the x,y,z
    of the 25 joints in
%   camera space coordinates
% - Orientation:
%   If input parameter is 'Quat': 4x25 matrix
    containing the
%   orientation of each joint in [x; y; z, w]
%   If input parameter is 'Euler': 3x25 matrix
    containing the
%   orientation of each joint in [Pitch; Yaw;
    Roll]
% -TrackingState: state of each joint. These
    can be:
%   NotTracked=0, Inferred=1, or Tracked=2
% -LeftHandState: state of the left hand
% -RightHandState: state of the right hand

[bodies, fcp, timeStamp] = k2.getBodies('Quat')
    ; % Viimeisimmän framen bodies-tiedot. The
    timestamp, when the fram was created in
    milliseconds

 % Draw bodies on depth image
% Parameters:
% 1) image axes
% 2) bodies structure
% 3) Destination image (depth or color)
% 4) Joints' size (circle raddii)
% 5) Bones' Thickness
% 6) Hands' Size
k2.drawBodies(d.ax,bodies,'depth',5,3,15); %
    The skeleton is drawn here: some fracture of
```

```
            seconds later than the first body data was
                collected

            % Draw bodies on color image
            k2.drawBodies(c.ax,bodies,'color',10,6,30);
%
%               end
%           end
            %save('tulos.mat','bodies');
            % Number of bodies detected
            numBodies = size(bodies,2);
            %disp(['Bodies Detected: ' num2str(numBodies)])

            % Example of how to extract information from
                getBodies output.
            if numBodies > 0
                % first body info:
                %disp(bodies(1).TrackingState)
                %disp(bodies(1).RightHandState)
                %disp(bodies(1).LeftHandState)

                %disp('Right Hand Orientation') % see Kin2.
                    m constants
                %disp(bodies(1).Orientation(:,k2.
                    JointType_HandRight));

                disp('Floor Clip Plane')
                disp(fcp);

                disp('Body Timestamp')
                disp(timeStamp);

                % To get the joints on depth image space,
                    you can use:
                %pos2D = k2.mapCameraPoints2Depth(bodies(1)
                    .Position');
            end
            % Laura Jukola
            % The first body frame instance is dealt with
                separately
```

```
        if n ==1 % When a body is tracked, it draws the
            skeleton first and still for one time asks
           for keypress to fill all conditions
            [~,~,button] = ginput(1); % Click on the
               image (1=left mouse button, 2=center
               button, 3=rigth mouse button)
            %Tracking will start, when the right mouse
               button is pressed
            %and a body has been tracked
            if (~isempty(bodies) && button == 3) % If
               body turns away, data is still not
               tracked because of this condition, then
               timepoint zero will be in the wrong
               place
%             if strcmp(w,'s');
                  %if n == 1
                  % Start the collection of
                     orientational data
                   systemCommand='python C:\Python27\
                      recv_streamer.py orientaatio2.
                      txt &'
                   system(systemCommand)
                      start = clock % Save the
                         timestamp of the first frame
                          of a succesfully tracked
                         body
                      tic
                  % If body was tracked
                  % Collecting 3D location data of
                     the right hand
                  hand_r(:,n) = bodies.Position(:,12)
                     ;
                  hand_l(:,n) = bodies.Position(:,8);
                  fwrite(s,'a'); % Command the
                     microcontroller to give send a
                     pulse
                  time_f(n) = toc; % Time of frames
                  % IMU data collection
                  n = n+1;
            end
        else % When n >1: just collect
```

```
            if(~isempty(bodies))
                hand_r(:,n) = bodies.Position(:,12);
                hand_l(:,n) = bodies.Position(:,8);
                time_f(n) = toc;
             n = n+1; % N number of frames collected
            end
        end
         %end
        % end

    % If user presses 'q', exit loop
    if ~isempty(k)
        if strcmp(k,'q'); break; end;
    end

    pause(0.02) % There needs to be a slight pause,
       otherwise there won't be enough time for the
       program to draw the skeletons
    %toc
    end
end
% Put down the voltage in arduino microcontroller
%fwrite(s,'b');
% Close the microcontroller
fclose(s);
% Close kinect object
k2.delete;

close all;
```

Appendix B

Collection of UDP packages sent by a smart phone

The Python-code for collecting UDP packages that contain orientation data collected from smart phones' gyroscope, accelerometer and teslameter:

```
import SocketServer
import time
import struct
import sys
import datetime

# Function collects UDP packages from a smartphone
    application called Sensor Streamer
if len(sys.argv) < 2:
     print "Filename argument missing!"
     exit()

PORTNO = 10552 # Create a port
file = open(sys.argv[1], "w") # Open the file, whose
    name was given as an argument
start_time = time.time() # Receive starting timestamp
    in epoch format in GMT time


alku = open("orientaatio2_start.txt","w")
alku.write("%f" % (start_time)) # Write the starting
    time in epoch-format to a tetx file
alku.close()
```

```
# Read the UDP package and unpack and sort the data
class handler(SocketServer.DatagramRequestHandler):
    def handle(self):
        newmsg = self.rfile.read() #self.rfile.readline
            ().rstrip()
        # print "Client %s said ``%s''" % (self.
            client_address[0], newmsg[0:2])
        # possible problem with byte order
        accx  = struct.unpack('f', newmsg[4:8])[0]
        accy  = struct.unpack('f', newmsg[8:12])[0]
        accz  = struct.unpack('f', newmsg[12:16])[0]
        gyrox = struct.unpack('f', newmsg[16:20])[0]
        gyroy = struct.unpack('f', newmsg[20:24])[0]
        gyroz = struct.unpack('f', newmsg[24:28])[0]
        magx = struct.unpack('d',  newmsg[28:36])[0]
        magy = struct.unpack('d',  newmsg[36:44])[0]
        magz = struct.unpack('d',  newmsg[44:52])[0]
        curr_time = time.time() - start_time  #
            Calculate the time point
        self.wfile.write(self.server.oldmsg)
        self.server.oldmsg = newmsg
        print("%f %f %f %f %f %f %f %f %f %f %f" % (
            start_time, curr_time, accx, accy, accz,
            gyrox, gyroy, gyroz, magx, magy, magz)) #
            Print the collected data
        file.write("%f %f %f %f %f %f %f %f %f %f %f\n" %
            (curr_time, accx, accy, accz, gyrox, gyroy,
            gyroz, magx, magy, magz)) # Write the
            collected data to a text file

s = SocketServer.UDPServer(('',PORTNO), handler) # Open
    an UDP-port
print "Awaiting UDP messages on port %d, storing to
    file %s" % (PORTNO, sys.argv[1])
s.oldmsg = "This is the starting message."
s.serve_forever() # Run until user interrupts
```

Appendix C

Controlling Arduino UNO microcontroller

Code for controlling the Arduino UNO -microcontroller:

```
void setup() {
  // open the serial port:
  Serial.begin(9600);
  pinMode(12, OUTPUT);
  pinMode(13, OUTPUT);

}

void loop() {
  // check for incoming serial data:
  if (Serial.available() > 0) {
    int inByte = Serial.read();
    if (inByte = 97) {
      digitalWrite(12, HIGH); // Induce the pulse
      digitalWrite(13, HIGH); // Switch on the LED
      delay(1000);
      digitalWrite(12, LOW); // Shutdown the pulse
      digitalWrite(13, LOW); // Shutdown the LED
    }

  }
}
```